*Supplement of*

# How well can satellite altimetry and firn models resolve Antarctic firn thickness variations?

**Maria T. Kappelsberger et al.**

**Correspondence:** Maria T. Kappelsberger (maria.kappelsberger@tu-dresden.de)
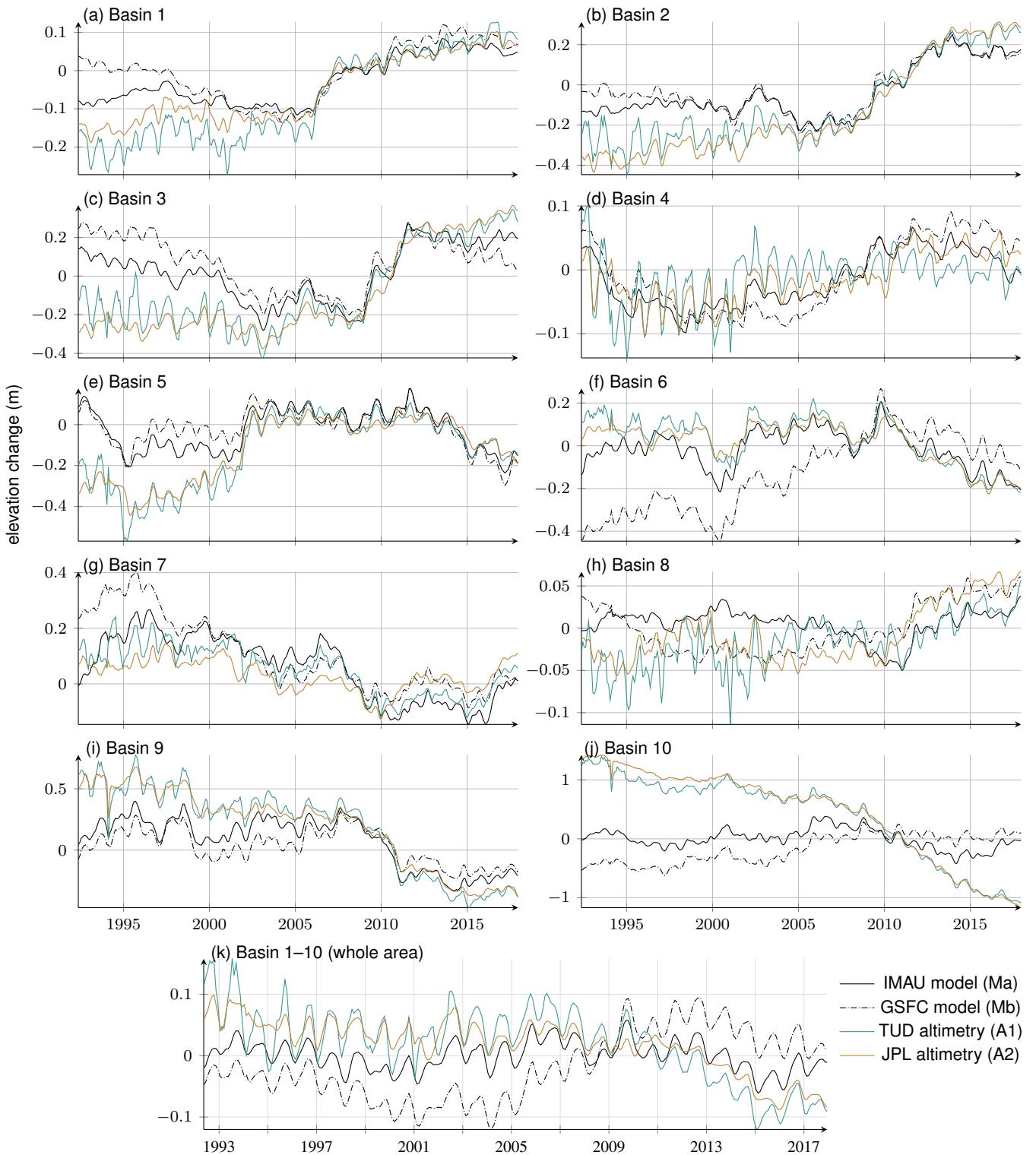
**Figure S1.** Basin mean time series of the original elevation changes from the IMAU firn model (Veldhuijsen et al., 2023), $h^{Ma}$, GSFC firn model (Medley et al., 2022), $h^{Mb}$, TUD altimetry (Schröder et al., 2019), $h^{A1}$, and JPL altimetry (Nilsson et al., 2022), $h^{A2}$.
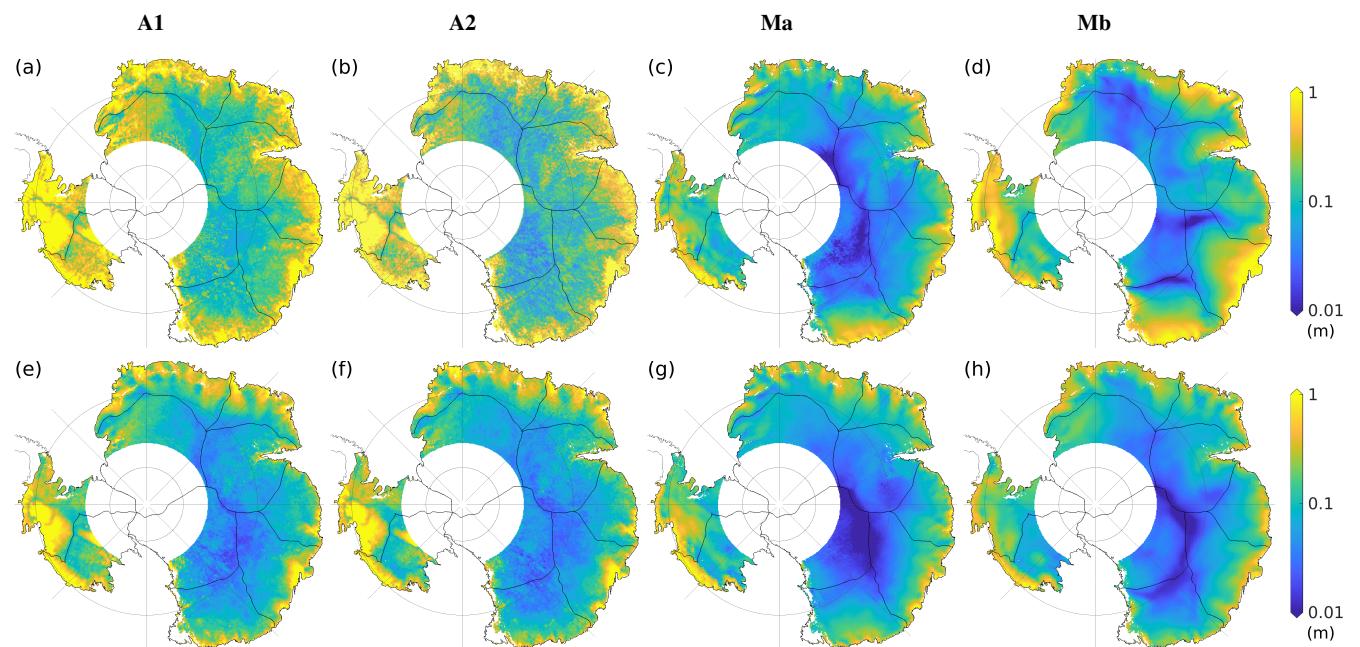
**Figure S2.** Root mean square (rms) of the original time series of elevation change over the period (a–d) before 2003 and (e–h) after 2003 for (a, e) TUD altimetry $h^{A1}$, (b, f) JPL altimetry $h^{A2}$, (c, g) the IMAU firn model $h^{Ma}$ and (d, h) the GSFC firn model $h^{Mb}$.
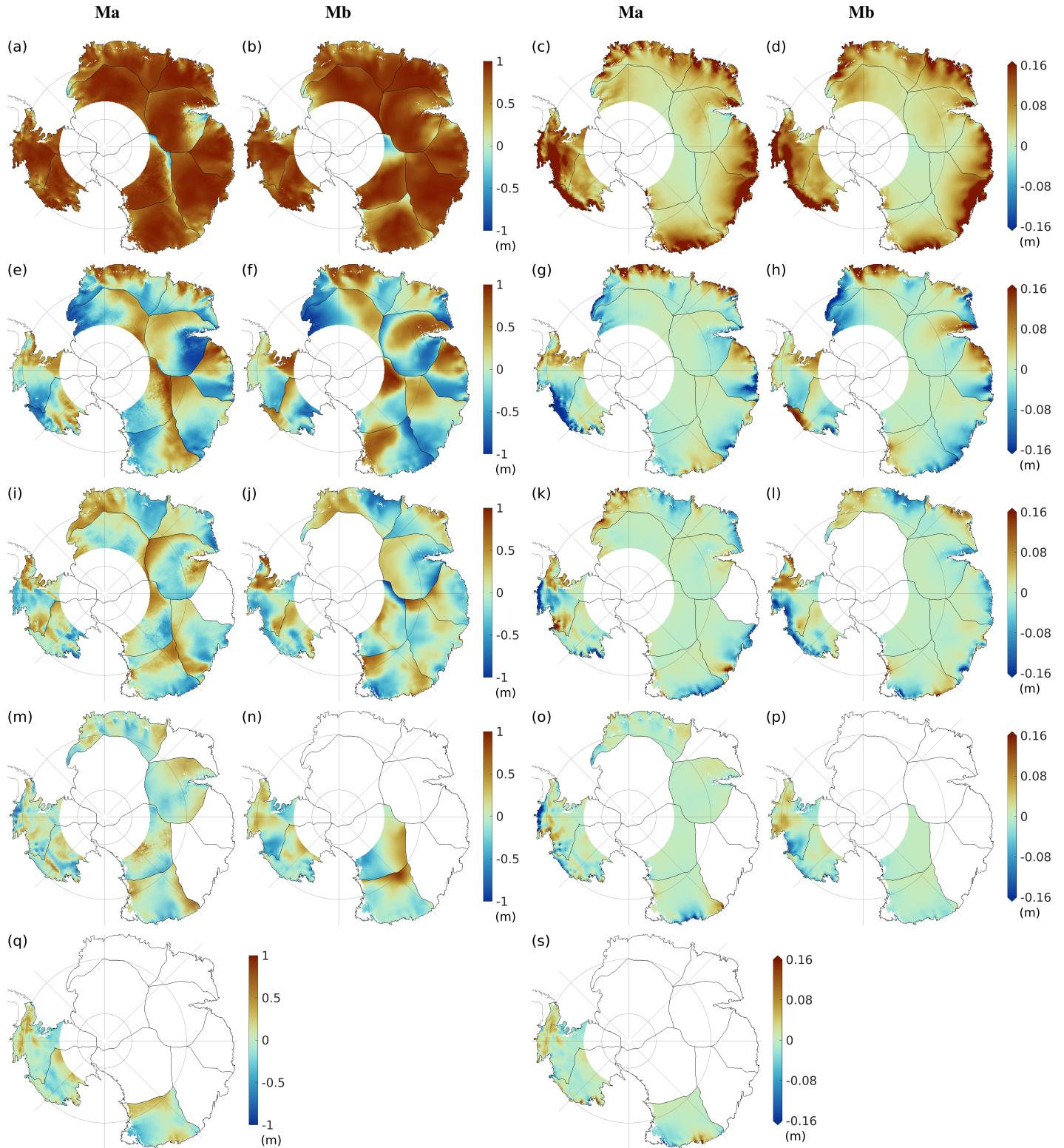
**Figure S3.** Dominant spatial patterns (EOFs) in firn thickness variations identified by the IMAU firn model (Ma, 1st column) and the GSFC firn model (Mb, 2st column). EOFs are derived from standardised modelling data (Section 3.1.1). 'Modelled' scaling factors $e^{M}_{1,...,5}$ adjusted to (non-standardised) monthly elevation changes from Ma (3rd column) and Mb (4th column). (a–d) First, (e–h) second, (i–l) third, (m–p) fourth and (q, s) fifth EOFs or rather scaling factors. The respective temporal patterns (PCs) are given by Fig. S4 and S5 for Ma and Fig. S6 and S7 for Mb, respectively.
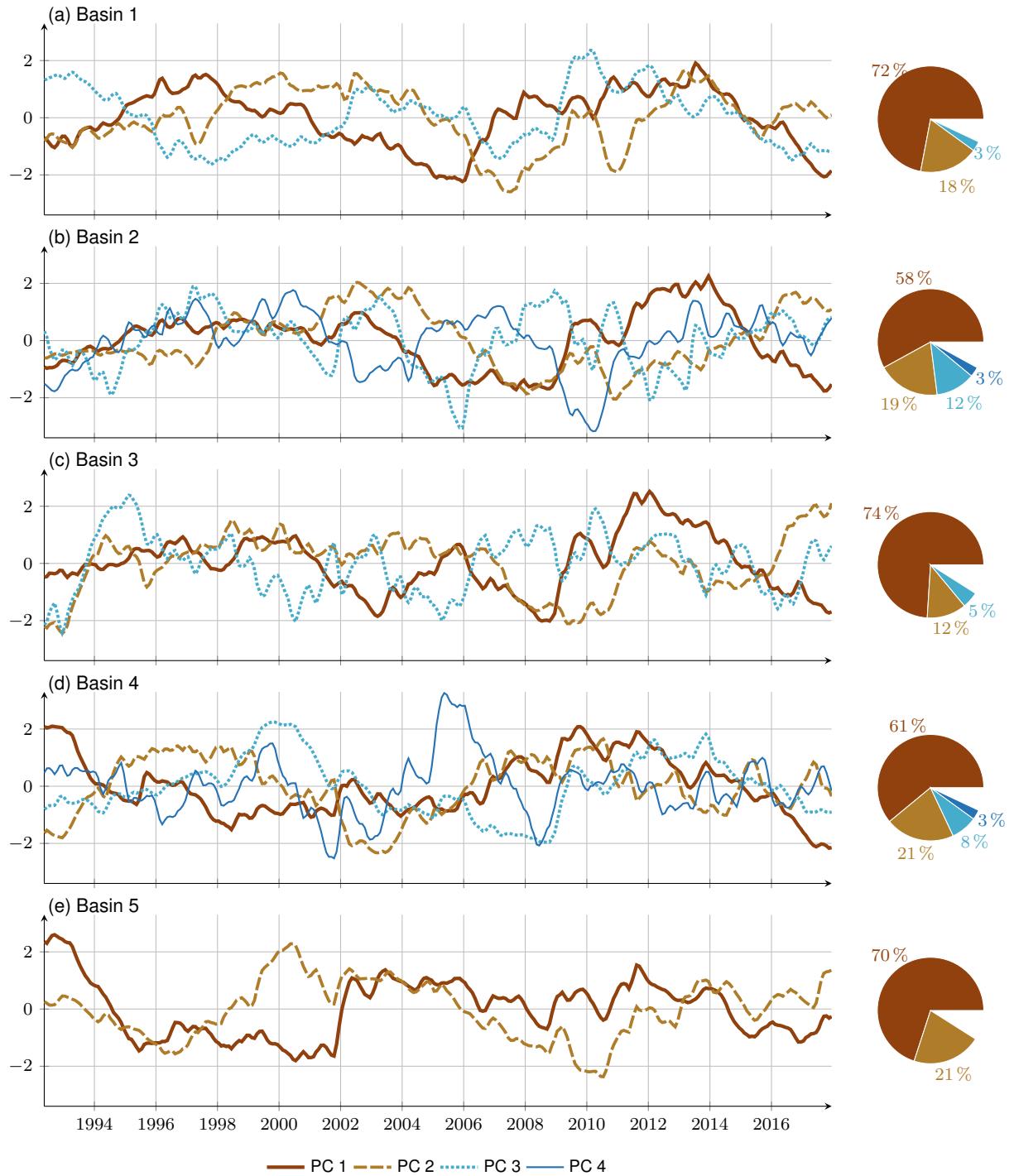
**Figure S4.** Dominant PCs in firn thickness variations identified by Ma for (a–d) basins 1–5 (line chart) and associated percentages of the basin's total data variance considering the respective PC/EOF pair (pie chart). The respective EOFs are given by Fig. S3 (1st column). We define the PCs as standardised time series (mean of zero, std of 1) and without a unit while the EOFs get the unit of meter.
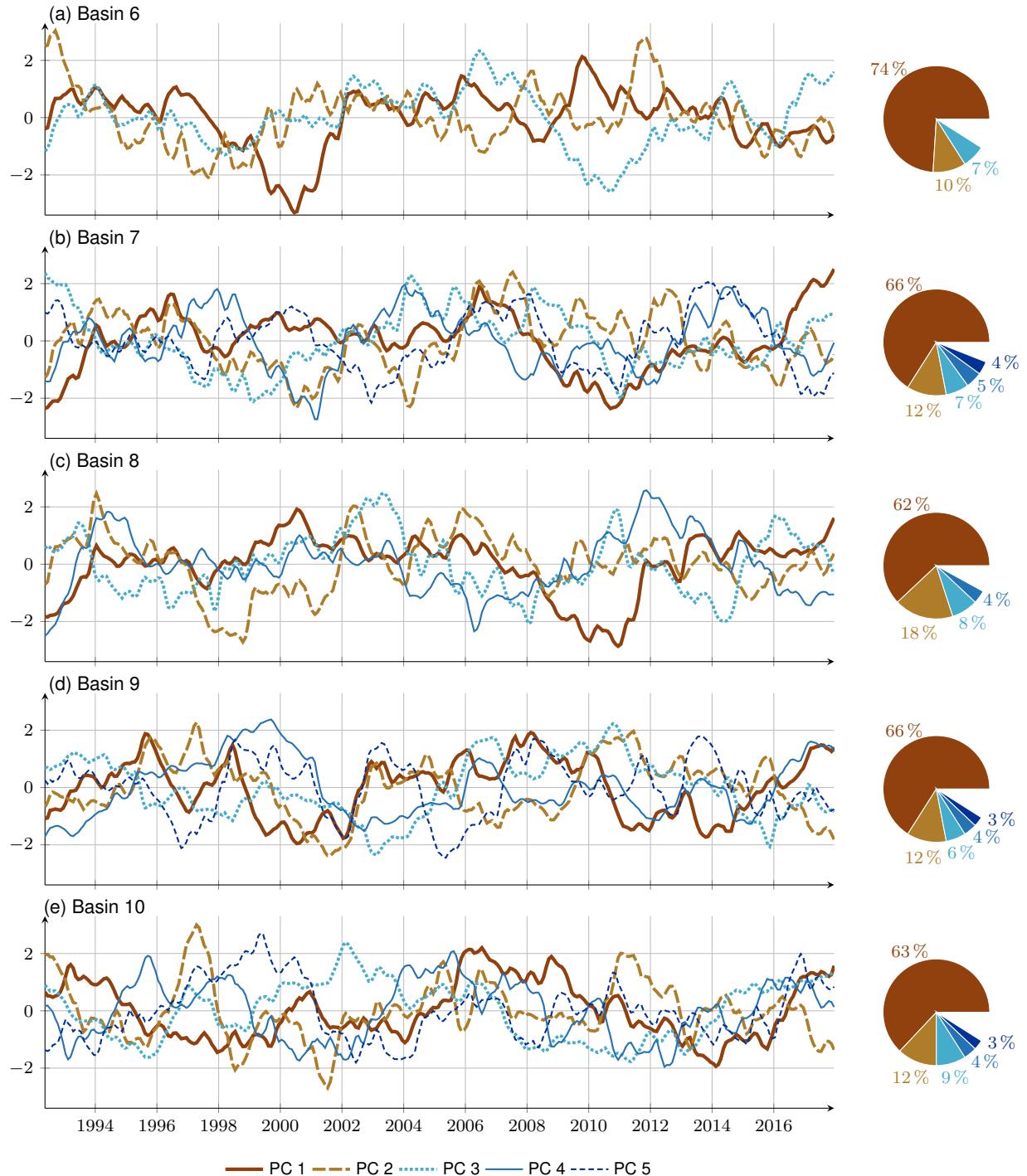
**Figure S5.** Dominant PCs in firn thickness variations identified by Ma for (a–d) basins 6–10 (line chart) and associated percentages of the basin's total data variance considering the respective PC/EOF pair (pie chart). The respective EOFs are given by Fig. S3 (1st column).
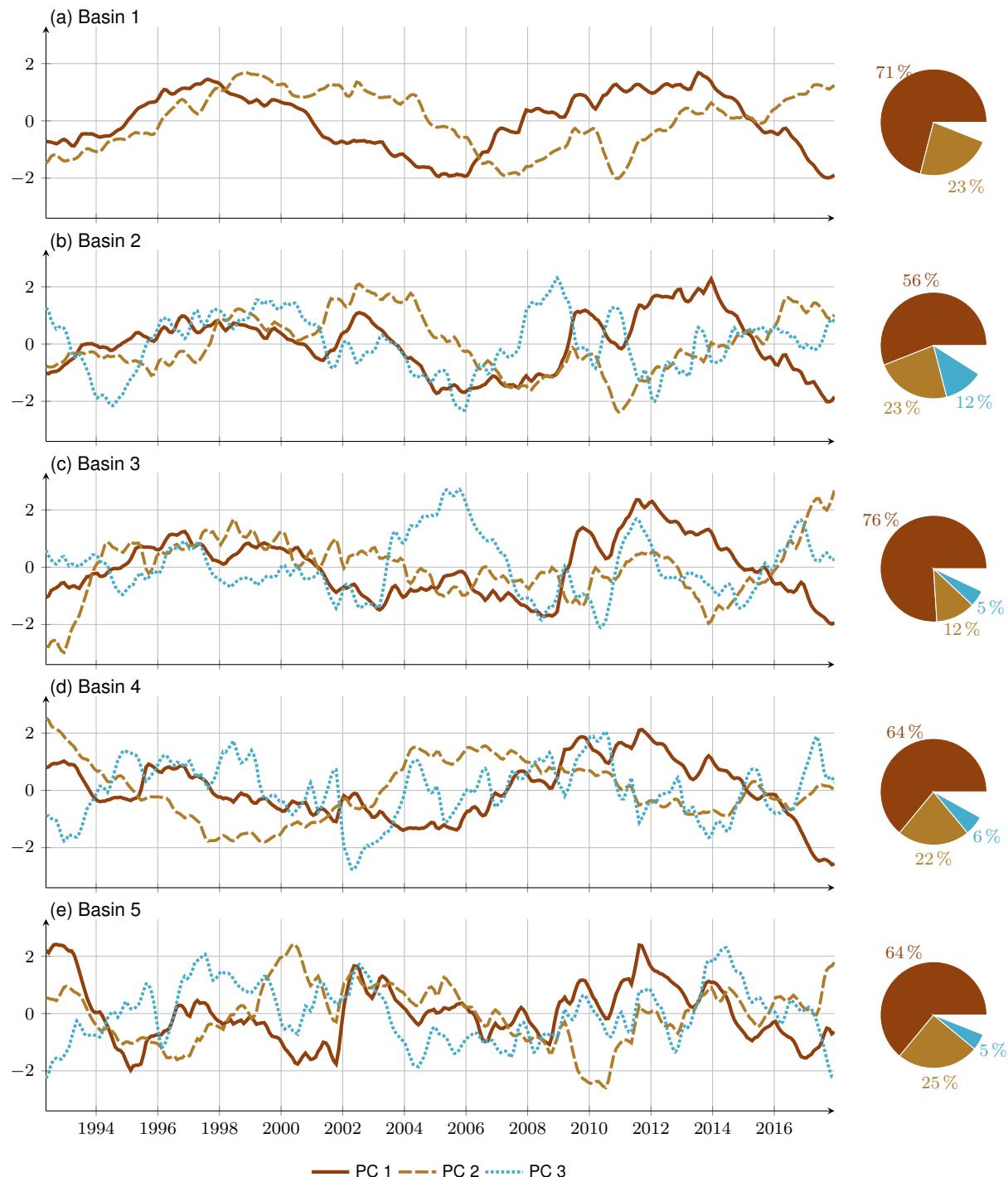
**Figure S6.** Dominant PCs in firn thickness variations identified by Mb for (a–d) basins 1–5 (line chart) and associated percentages of the basin's total data variance considering the respective PC/EOF pair (pie chart). The respective EOFs are given by Fig. S3 (2nd column).
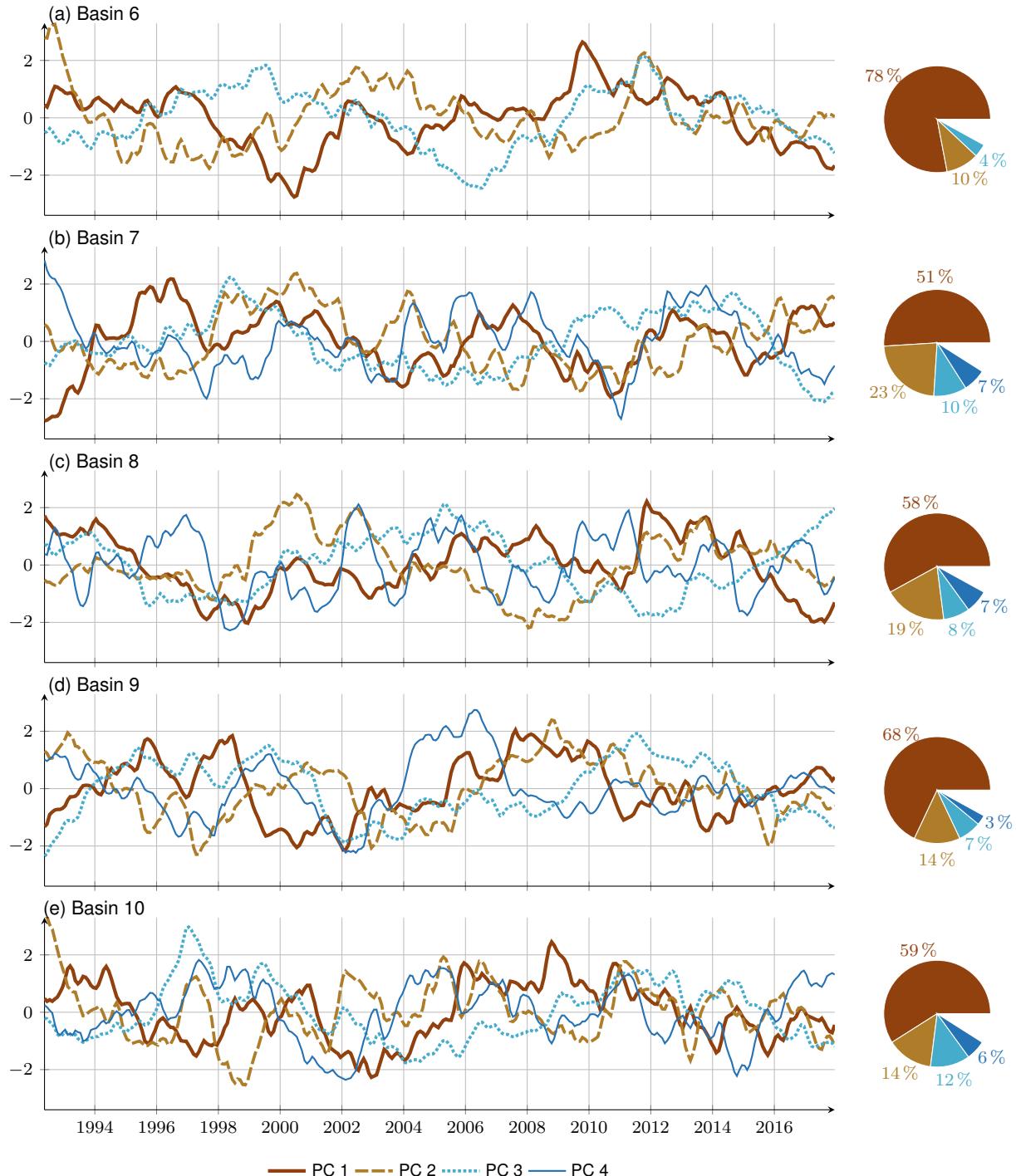
**Figure S7.** Dominant PCs in firn thickness variations identified by Mb for (a–d) basins 6–10 (line chart) and associated percentages of the basin's total data variance considering the respective PC/EOF pair (pie chart). The respective EOFs are given by Fig. S3 (2nd column).
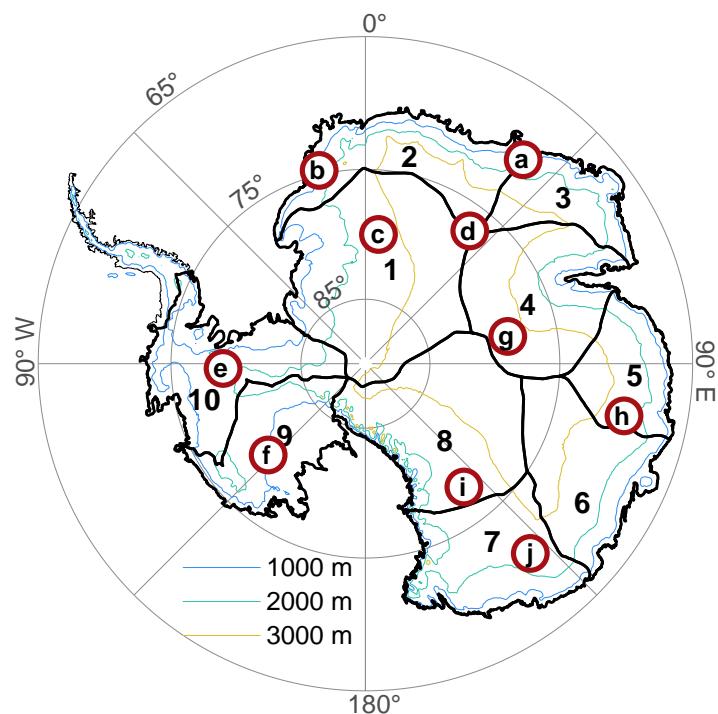
**Figure S8.** Subset of selected grid points a–j. Their locations were taken from Veldhuijsen et al. (2023) Fig. 9. Additionally the (aggregated) drainage basins of the East and West AIS used in this study (thick black lines) following Rignot et al. (2011a, b) and the contour lines of the ice sheet surface are shown.
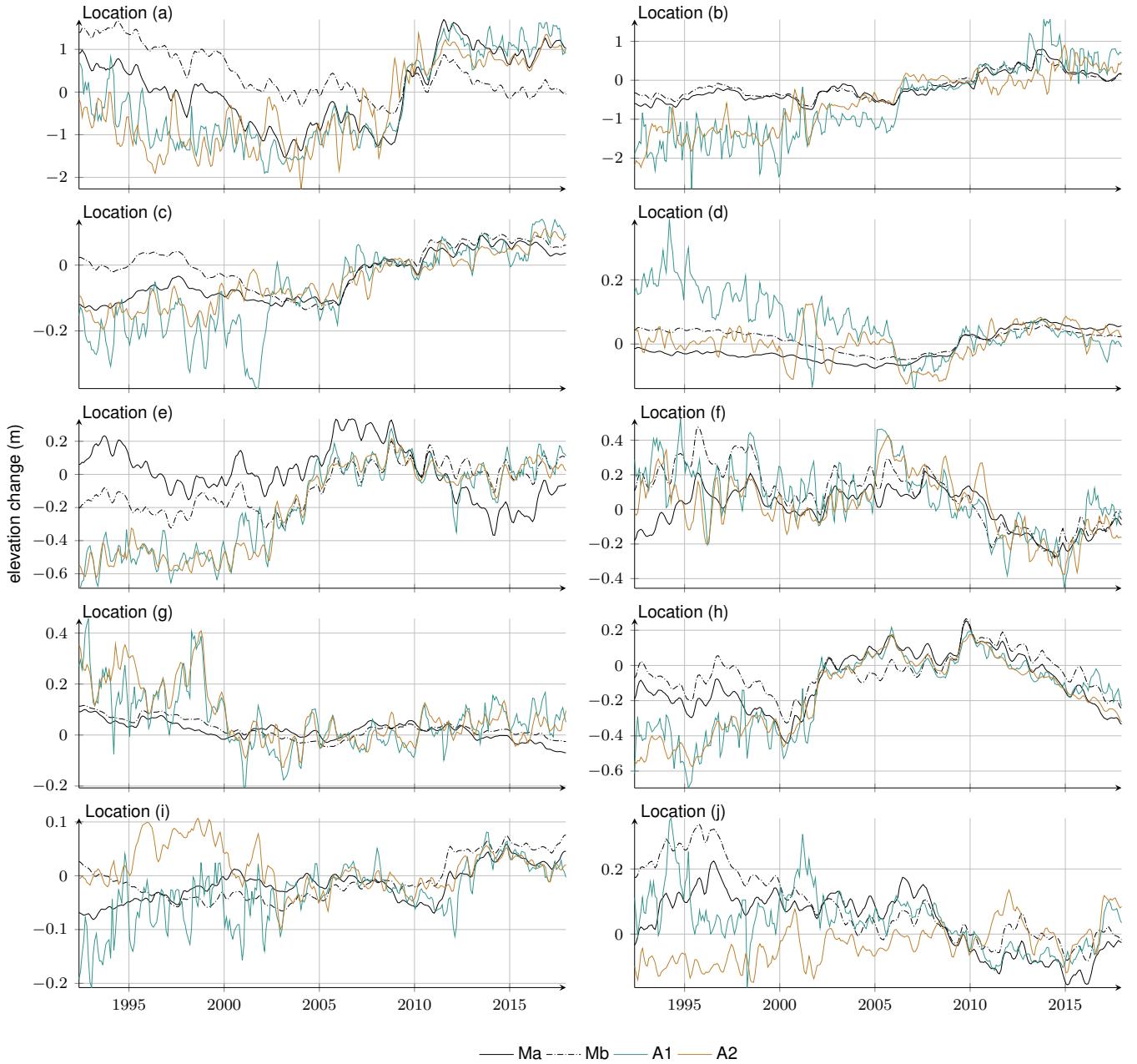
**Figure S9.** Time series of the original elevation changes ($h^{Ma}$, $h^{Mb}$, $h^{A1}$, $h^{A2}$) for the subset of selected grid points a–j (Fig. 8).
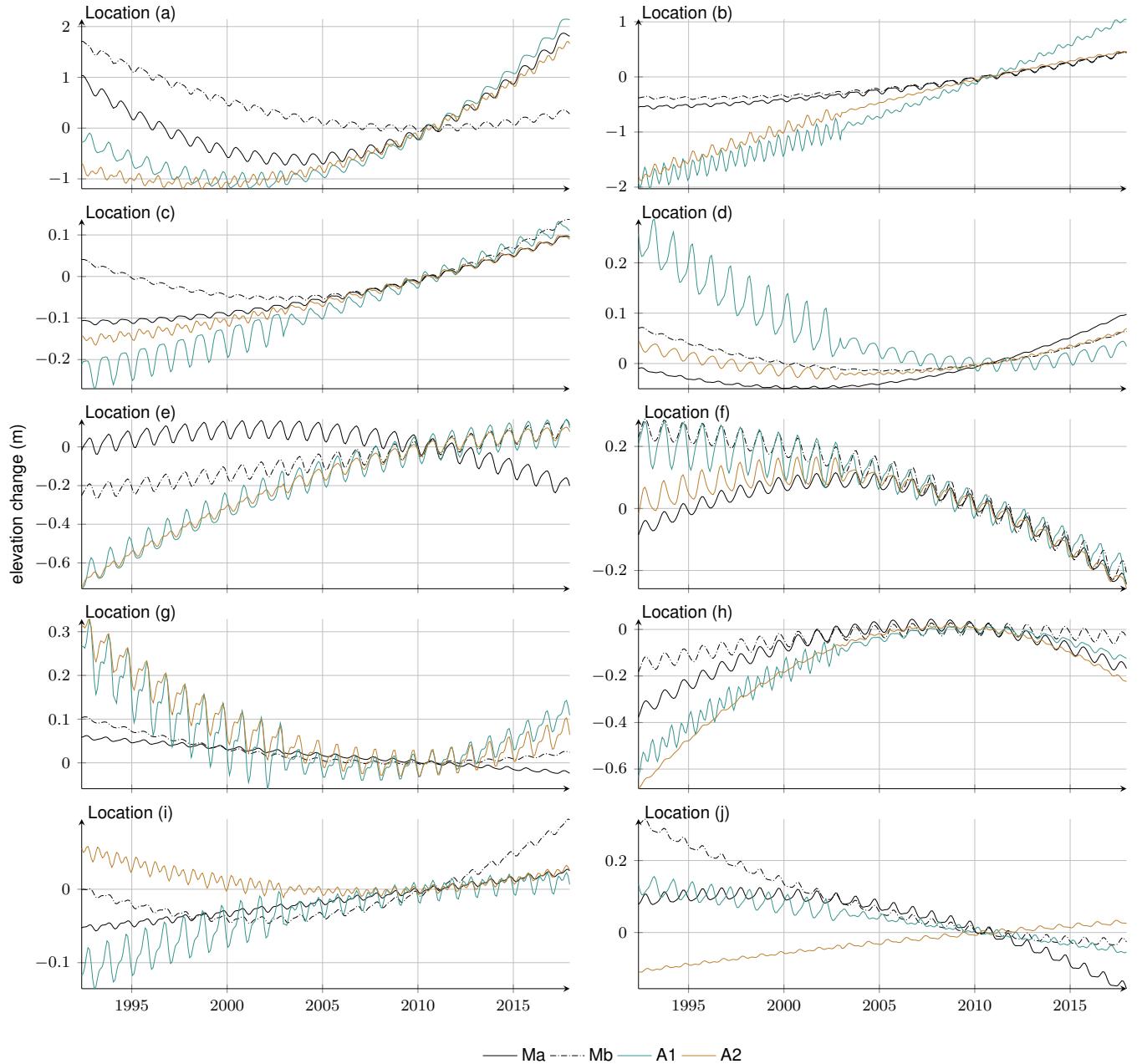
**Figure S10.** Time series of the adjusted linear, quadratic and seasonal model (based on Ma, Mb, A1, A2) for the subset of selected grid points a–j (Fig. 8).
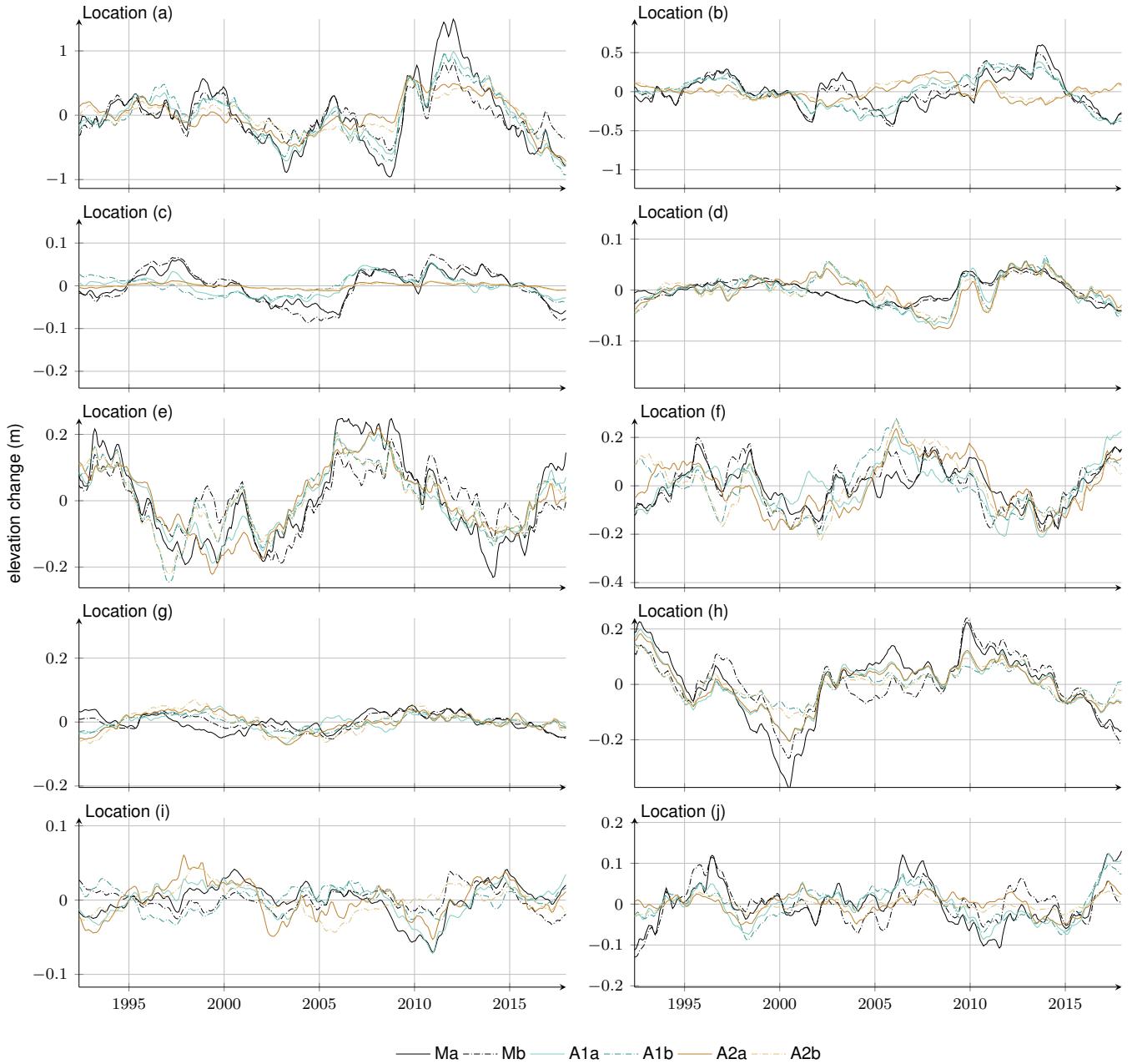
**Figure S11.** Time series of the modelled and adjusted firn thickness variations ($fv^{\text{Ma}}$, $fv^{\text{Mb}}$ and $fv^{\text{A1a}}$, $fv^{\text{A2a}}$, $fv^{\text{A1b}}$, $fv^{\text{A2b}}$) for the subset of selected grid points a–j (Fig. 8).
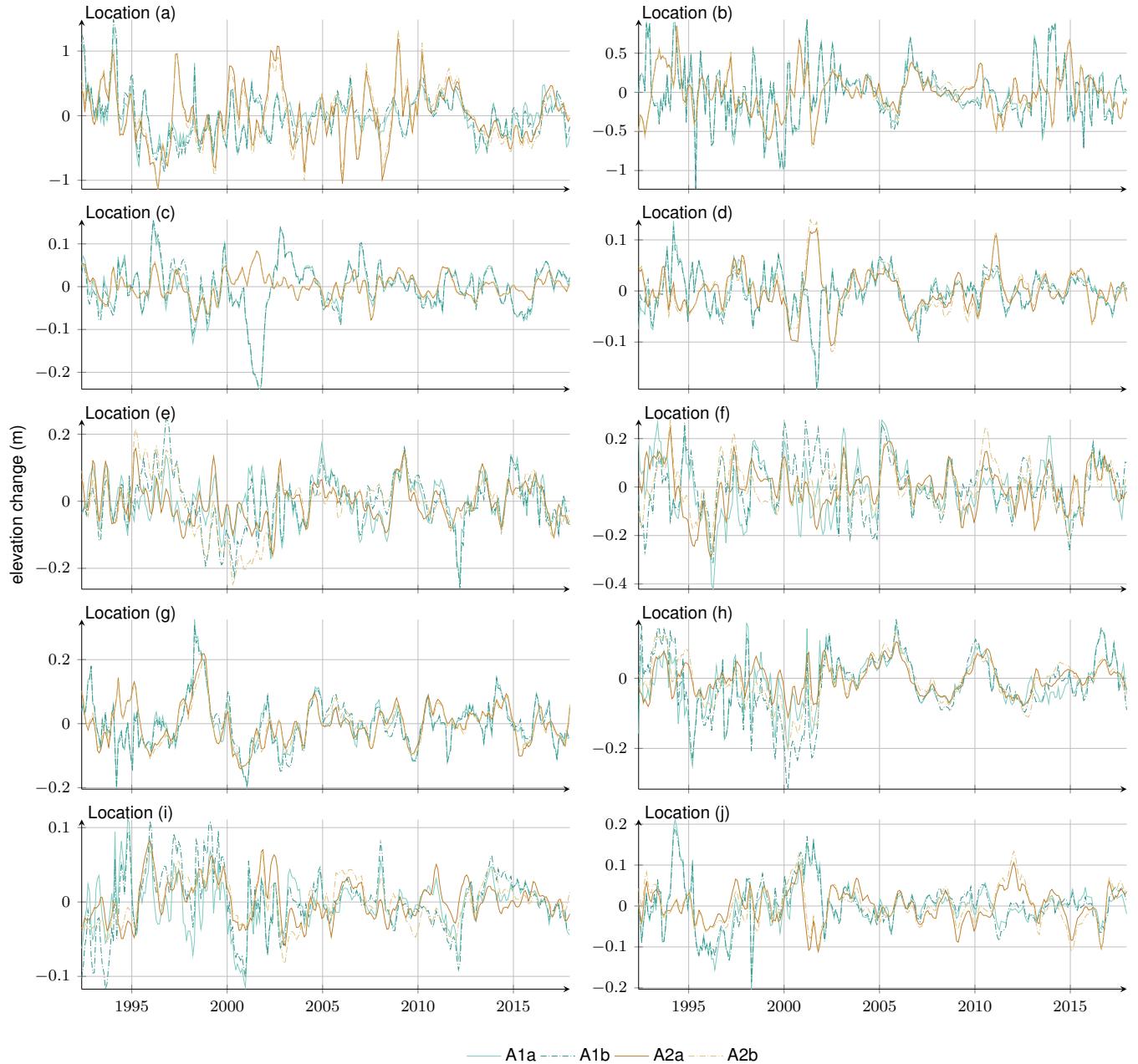
**Figure S12.** Time series of the altimetric residuals ($r^{A1a}$, $r^{A2a}$, $r^{A1b}$, $r^{A2b}$) for the subset of selected grid points a–j (Fig. 8).
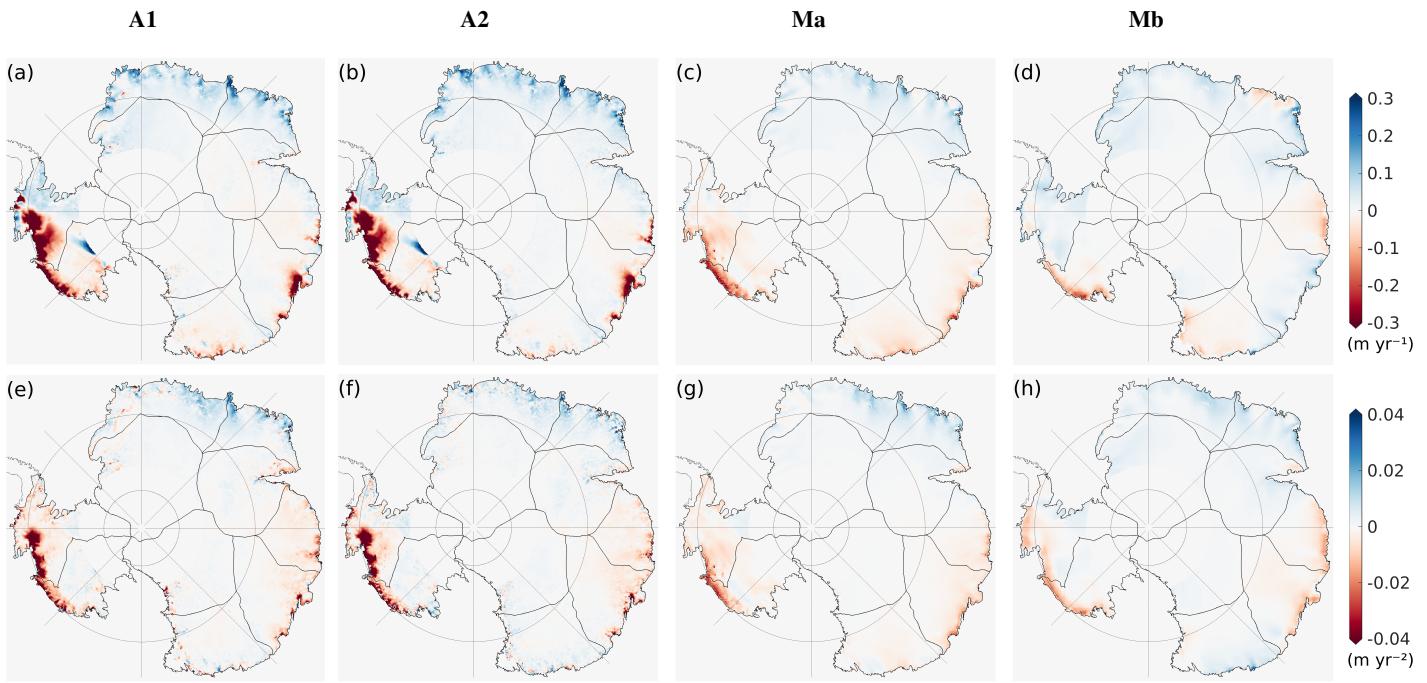
**Figure S13.** Adjusted regression parameters. (a–d) Linear and (e–h) quadratic terms adjusted to monthly elevation changes from (a, e) TUD altimetry (A1, 1st column), (b, f) JPL altimetry (A2, 2nd column), (c, g) IMAU firn model (Ma, 3rd column) and (d, h) GSFC firn model (Mb, 4th column).
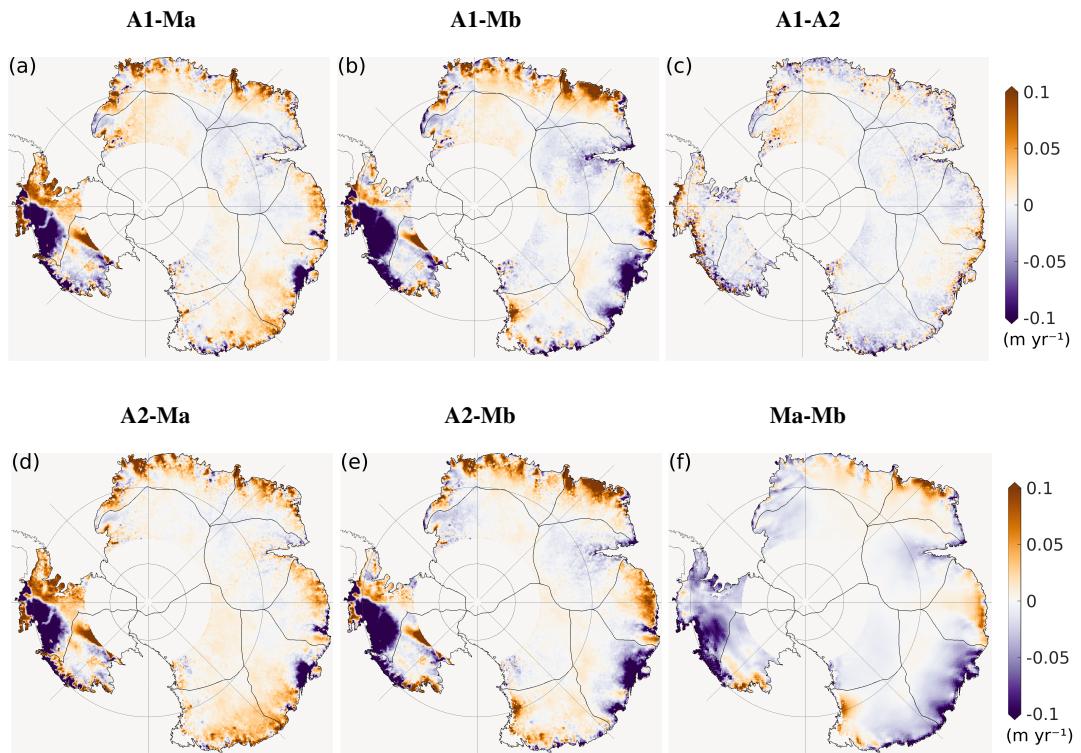
**Figure S14.** Differences in the adjusted linear terms.
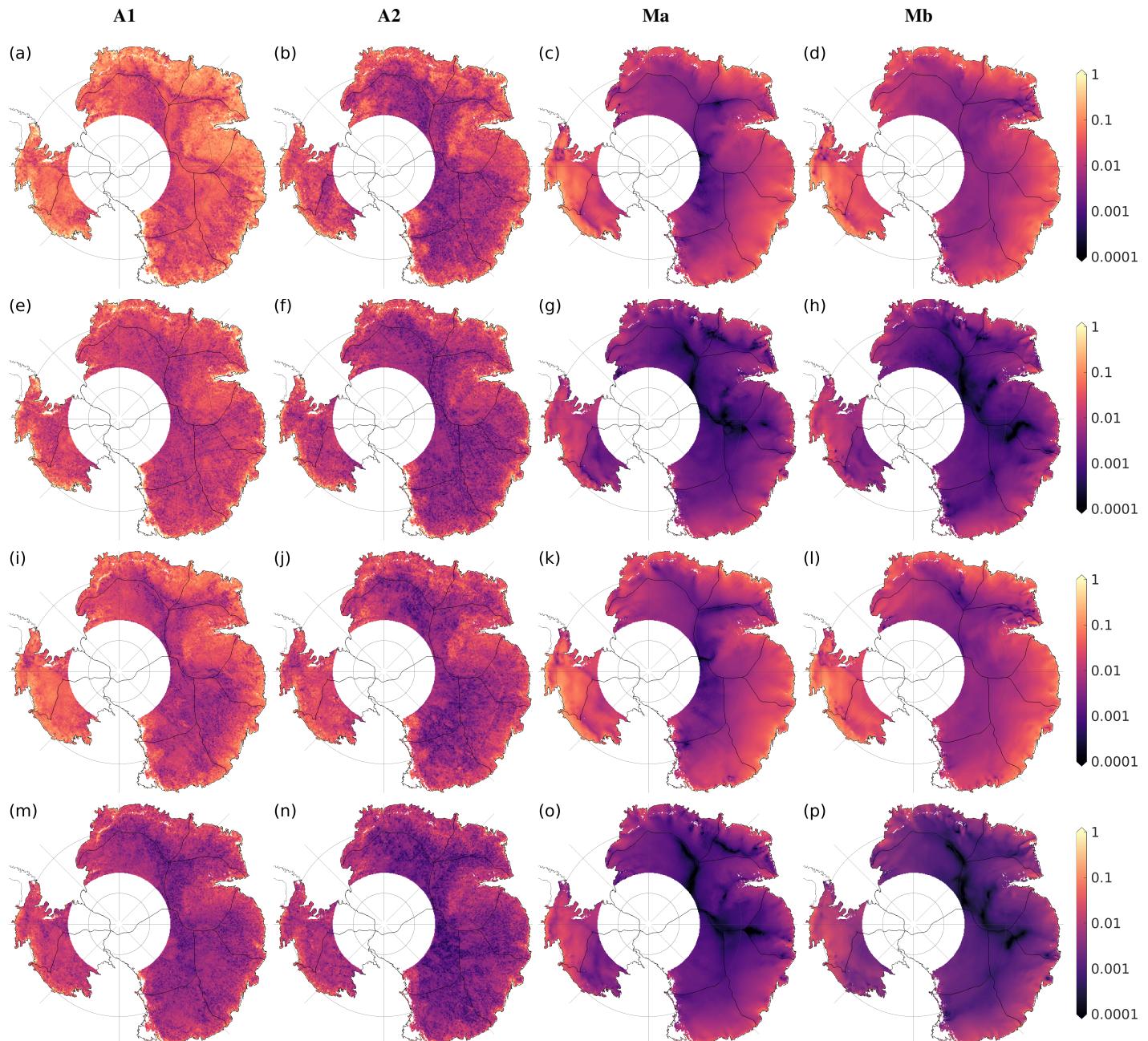
**Figure S15.** Adjusted regression parameters. (a–d) Annual amplitude before 2003, (e–h) semi-annual amplitude before 2003, (i–l) annual amplitude after 2003 and (m–p) semi-annual amplitude after 2003 adjusted to monthly elevation changes from A1 (1st column), A2 (2nd column), Ma (3rd column) and Mb (4th column).
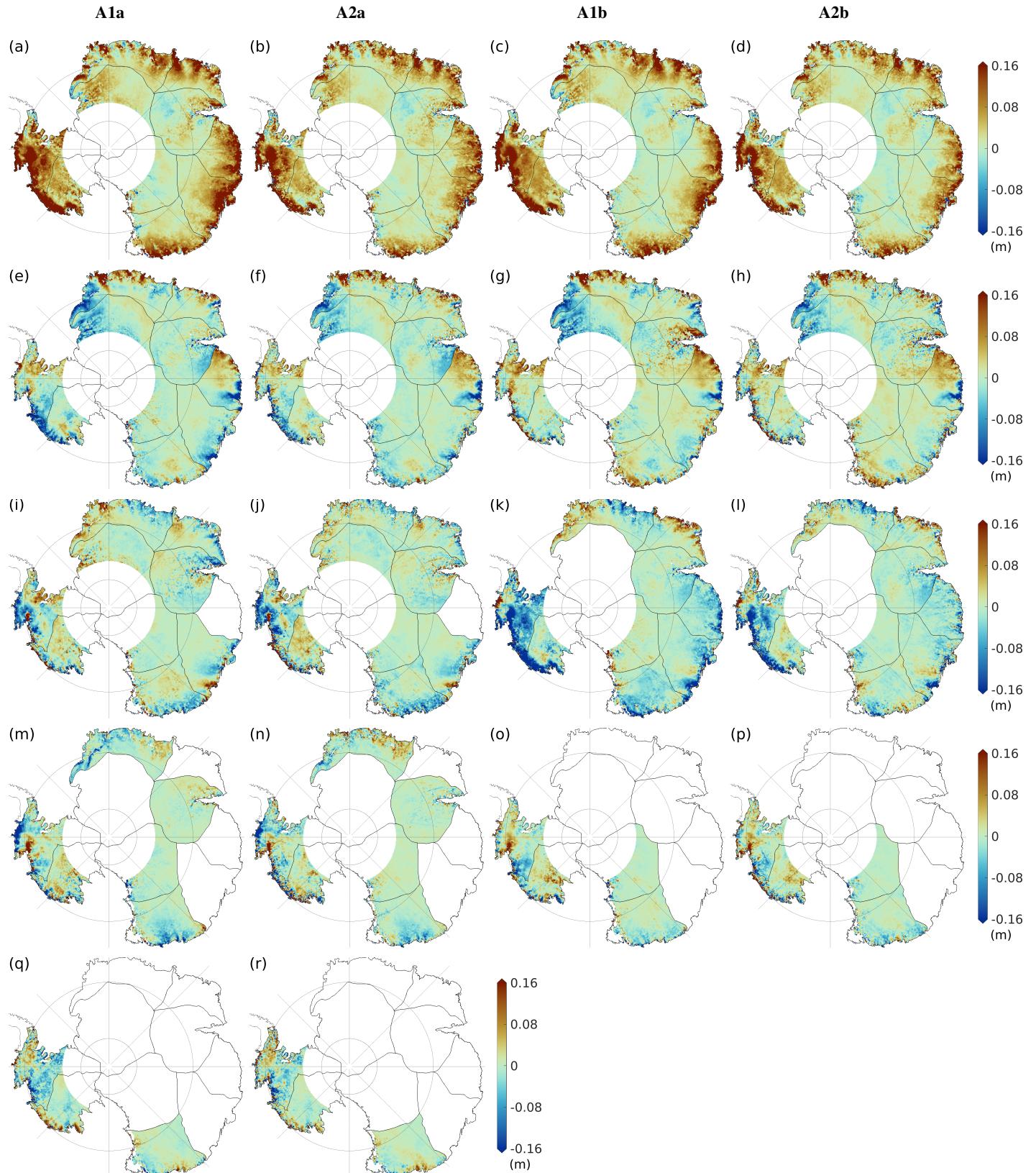
**Figure S16.** Adjusted regression parameters. 'Observed' scaling factors $e^{A}_{1,...,5}$ adjusted to monthly elevation changes from altimetry. Scaling factors given for (a–d) $h^{PC}_1$, (e–h) $h^{PC}_2$, (i–l) $h^{PC}_3$, (m–p) $h^{PC}_4$ and (q–r) $h^{PC}_5$ based on the four different versions: A1a (1st column), A2a (2nd column), A1b (3th column) and A2b (4th column). $e^{A}_{1,...,5}$ can be directly compared to $e^{M}_{1,...,5}$ (Fig. 3 columns 3 and 4).
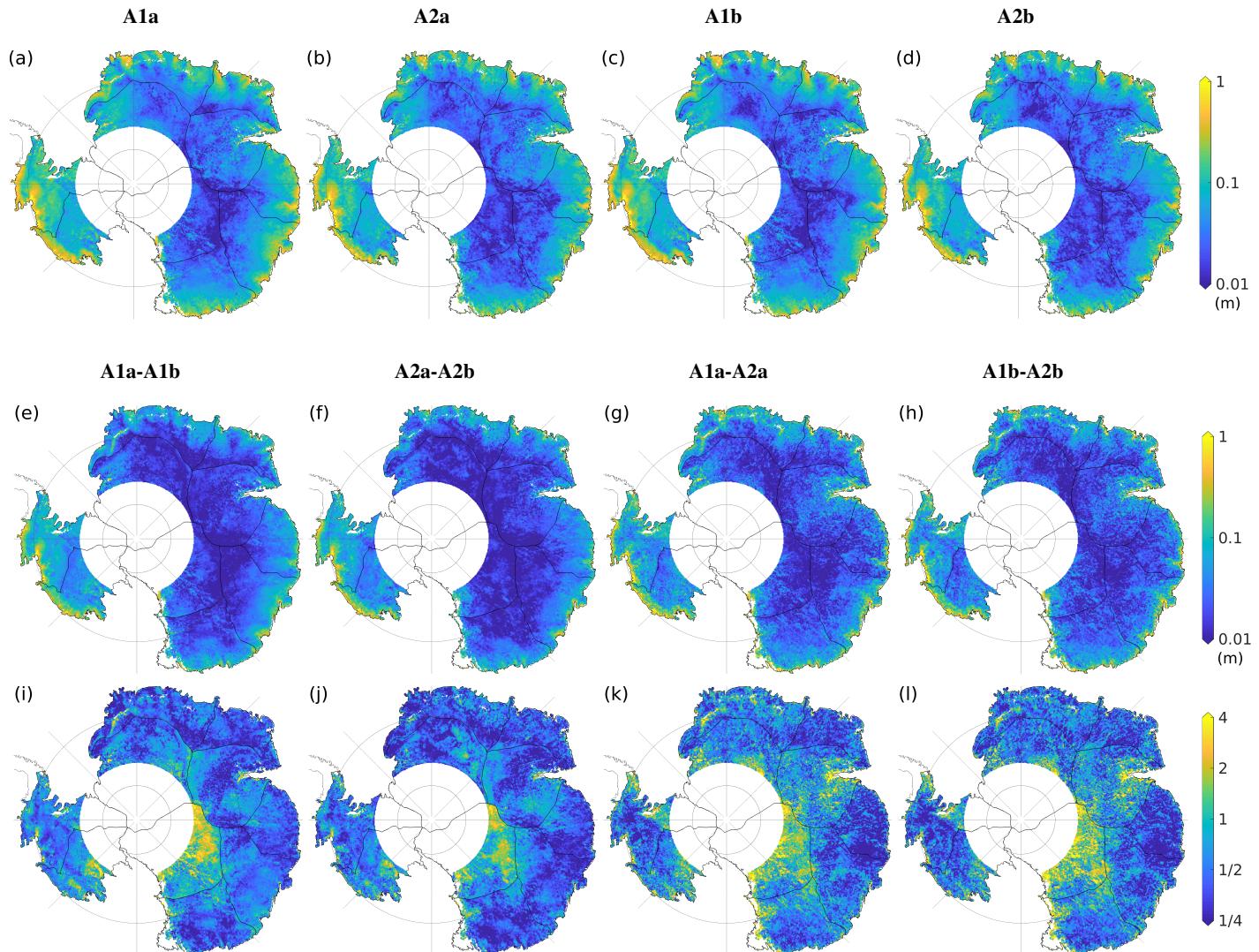
**Figure S17.** (a–d) Rms of the time series of adjusted firn thickness variations for the four different versions: (a) $fv^{\mathrm{A1a}}$, (b) $fv^{\mathrm{A2a}}$, (c) $fv^{\mathrm{A1b}}$ and (d) $fv^{\mathrm{A2b}}$. (e–l) Rms of the time series of their differences shown (e–h) absolutely and (i–l) relatively by normalising with the rms of $fv^{\mathrm{Ma}}$.
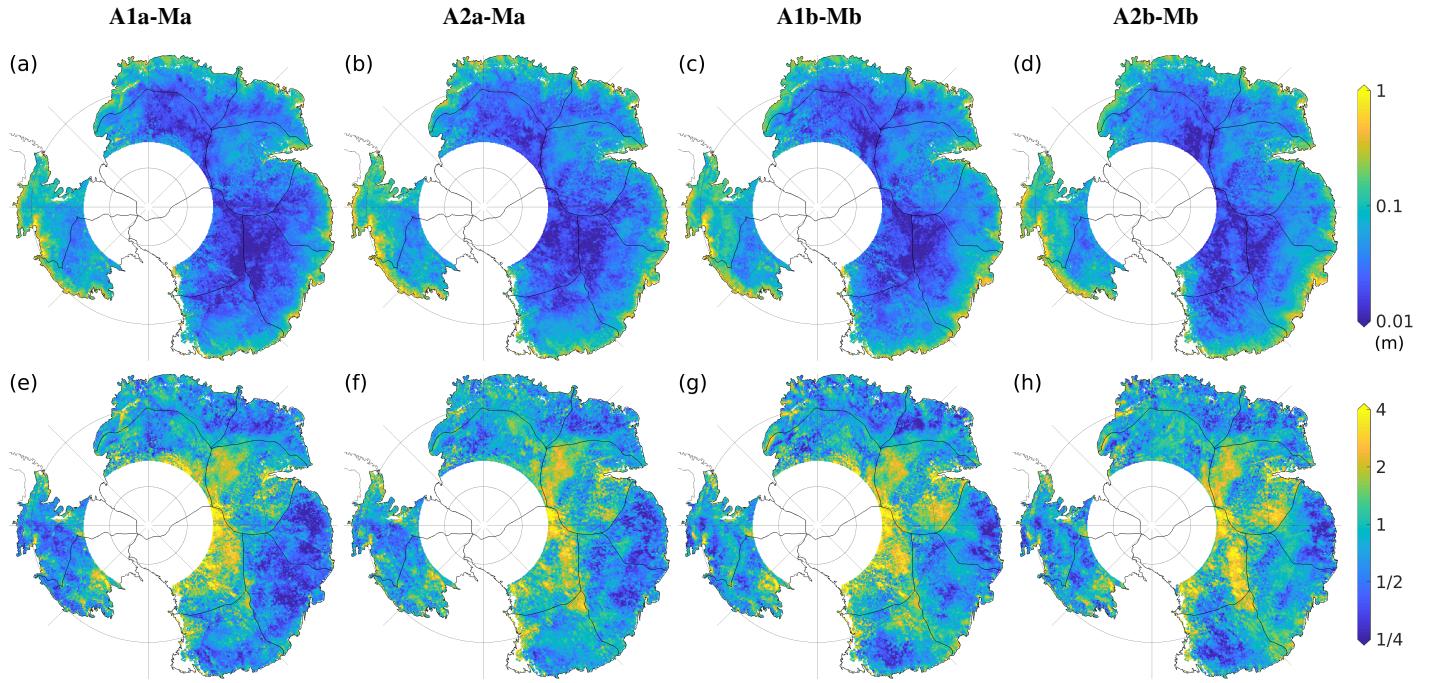
**Figure S18.** Rms of the time series of differences between adjusted and modelled firn thickness variations ($fv^{\mathrm{A}} - fv^{\mathrm{M}}$) shown (a–d) absolutely and (e–h) relatively by normalising with the rms of $fv^{\mathrm{Ma}}$.
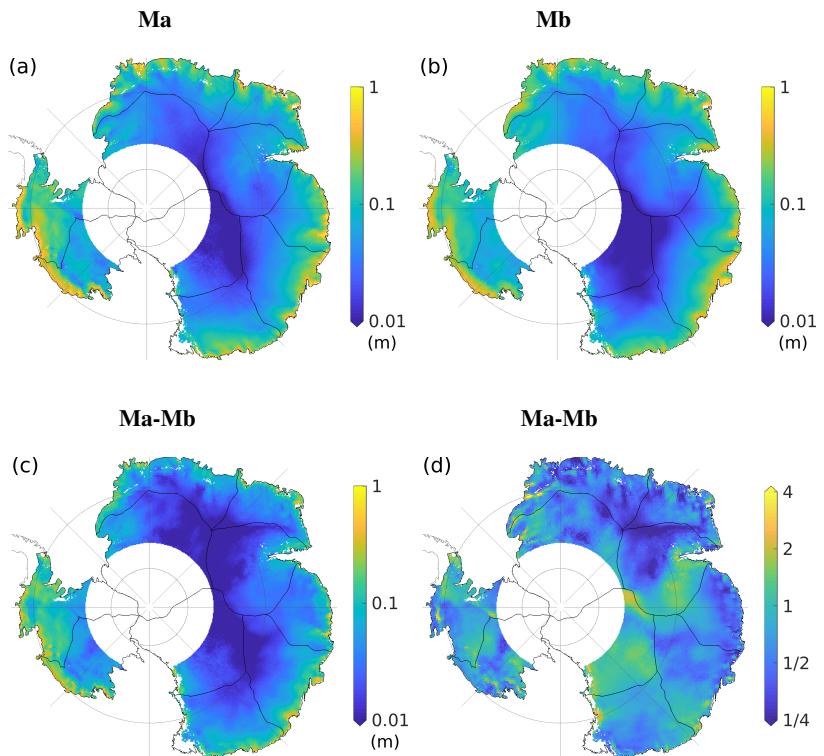
**Figure S19.** (a–b) Rms of the time series of modelled firn thickness variations for the two different models: (a) $fv^{\mathrm{Ma}}$ and (b) $fv^{\mathrm{Mb}}$. (c–d) Rms of the time series of their difference shown (c) absolutely and (d) relatively by normalising with the rms of $fv^{\mathrm{Ma}}$.
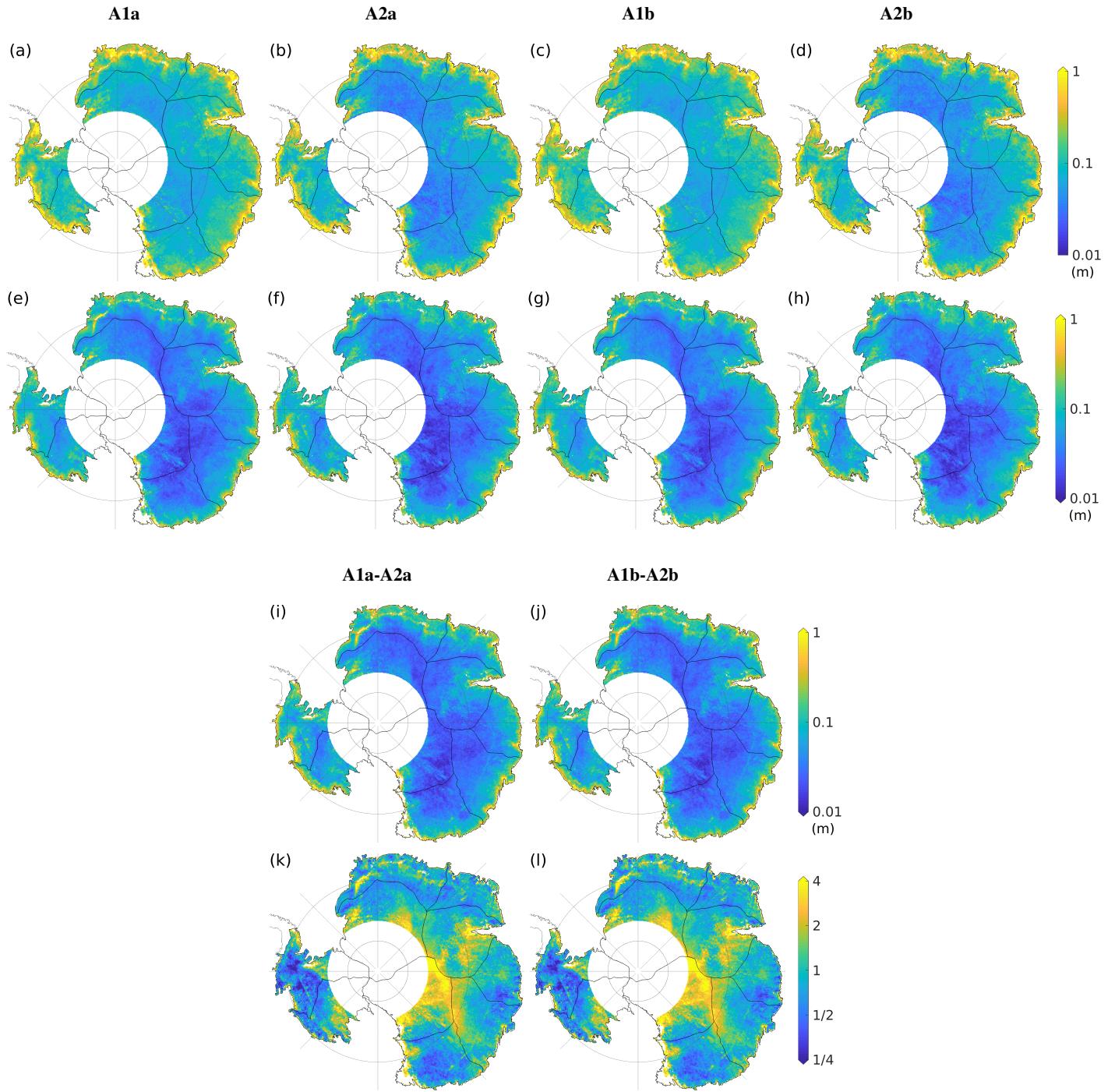
**Figure S20.** (a–h) Rms of the residual altimetric time series for the four different versions over the period (a–d) before 2003 and (e–h) after 2003. (e–h) Rms of the time series of their differences ($r^{A1} - r^{A2}$) w.r.t. the period after 2003 shown (e–f) absolutely and (g–h) relatively by normalising with the rms of $fv^{Ma}$.

**A1a**  **A2a**  **A1b**  **A2b**
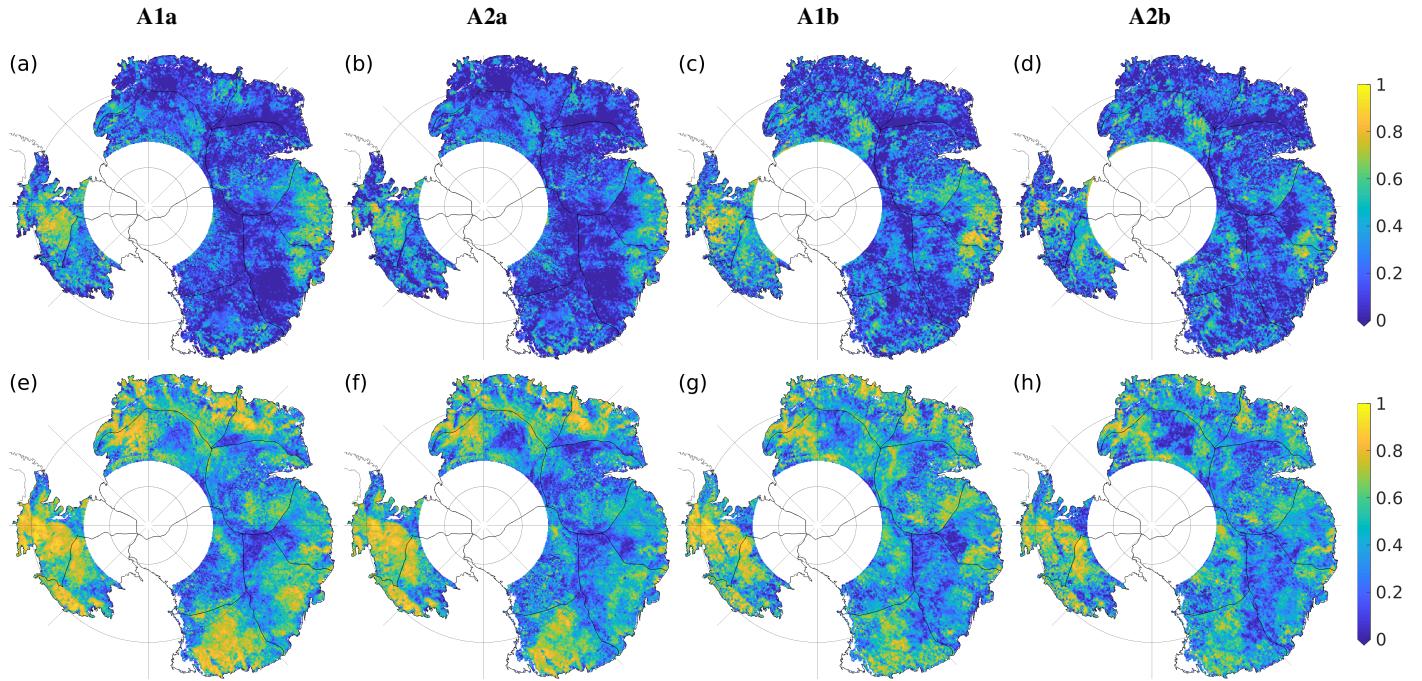
**Figure S21.** Coefficients of determination, $R_s$ for the four different versions of regression over the period (a–d) before 2003 and (e–h) after 2003.

**Table S1.** Explained variance or coefficients of determination, $R_s$, for each basin and each version of regression (Table 1) over the period before 2003. Apart from the last column $\overline{\text{A1a}}$, $R_s$ is first calculated for each grid cell according to Eq. 5a and after averaged over each basin. Values of $\overline{\text{A1a}}$ are calculated by first averaging the regression results over each basin and after applying Eq. 5a.

| Basin | A1a | A2a | A1b | A2b | $\overline{\text{A1a}}$ |
|---|---|---|---|---|---|
| 01 | 0.22 | 0.25 | 0.19 | 0.23 | 0.38 |
| 02 | 0.12 | 0.17 | 0.07 | 0.13 | 0.34 |
| 03 | 0.11 | 0.13 | 0.09 | 0.12 | 0.51 |
| 04 | 0.16 | 0.18 | 0.15 | 0.18 | 0.39 |
| 05 | 0.38 | 0.42 | 0.27 | 0.26 | 0.89 |
| 06 | 0.11 | 0.19 | 0.11 | 0.17 | 0.41 |
| 07 | 0.15 | 0.16 | 0.15 | 0.15 | 0.34 |
| 08 | 0.13 | 0.13 | 0.10 | 0.19 | -0.10 |
| 09 | 0.30 | 0.37 | 0.20 | 0.33 | 0.50 |
| 10 | 0.46 | 0.44 | 0.31 | 0.31 | 0.86 |
| 01–10* | 0.21 | 0.24 | 0.17 | 0.21 | 0.43 |

* refers to the entire area (considered as a single basin)
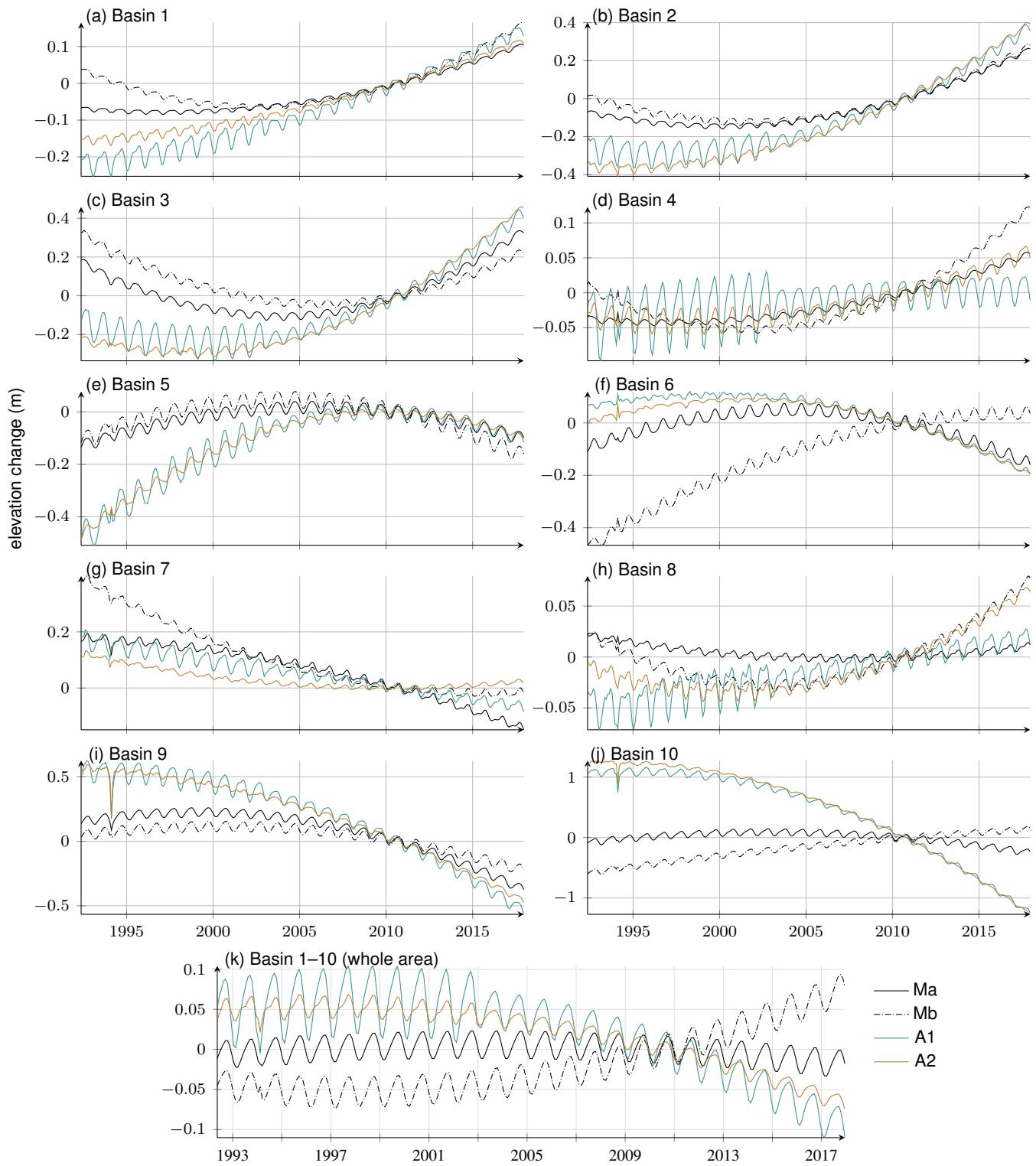
**Figure S22.** Basin mean time series of the adjusted linear, quadratic and seasonal model (based on Ma, Mb, A1, A2).
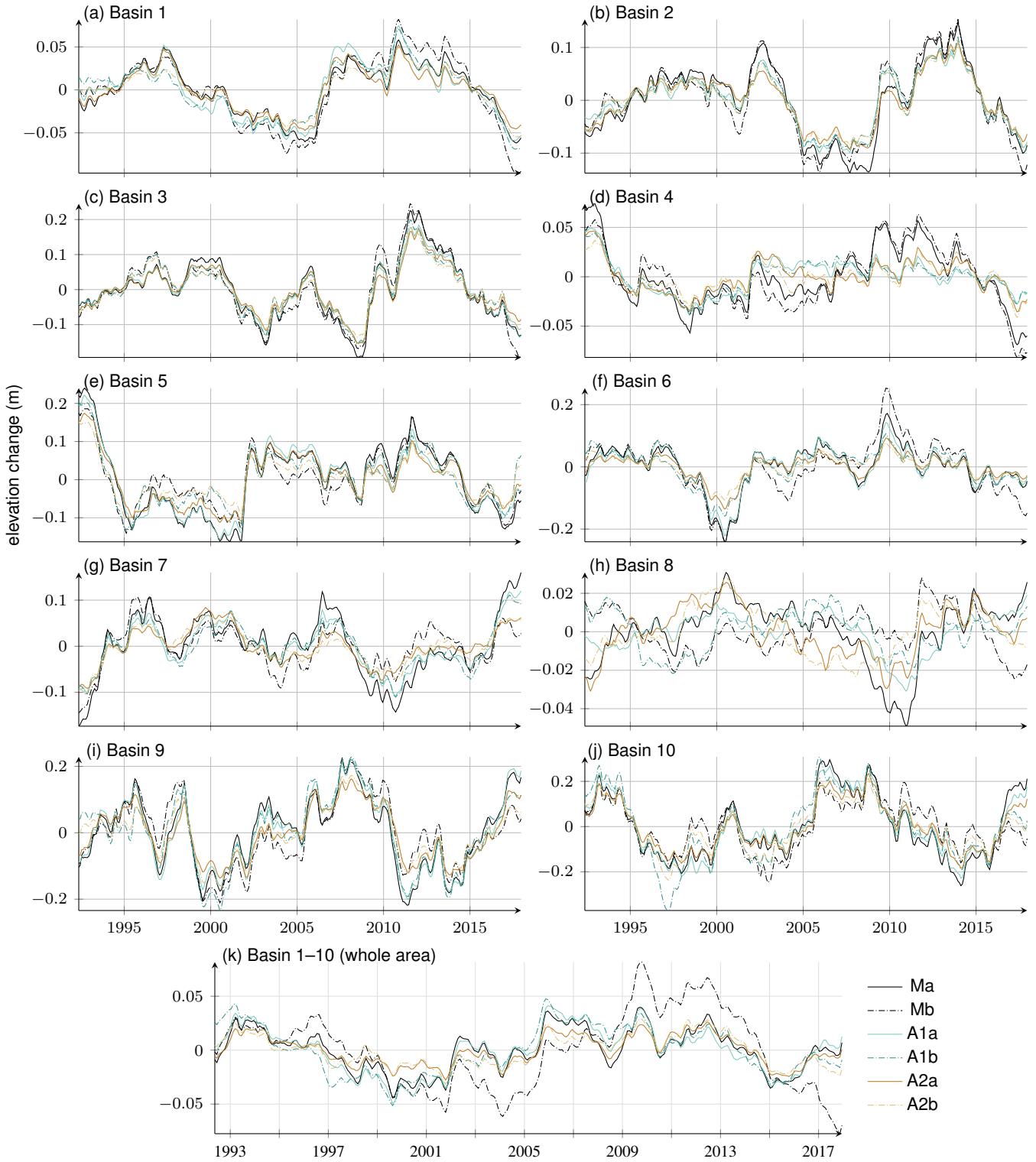
**Figure S23.** Basin mean time series of the modelled and adjusted firn thickness variations ($fv^{\text{Ma}}$, $fv^{\text{Mb}}$ and $fv^{\text{A1a}}$, $fv^{\text{A2a}}$, $fv^{\text{A1b}}$, $fv^{\text{A2b}}$).
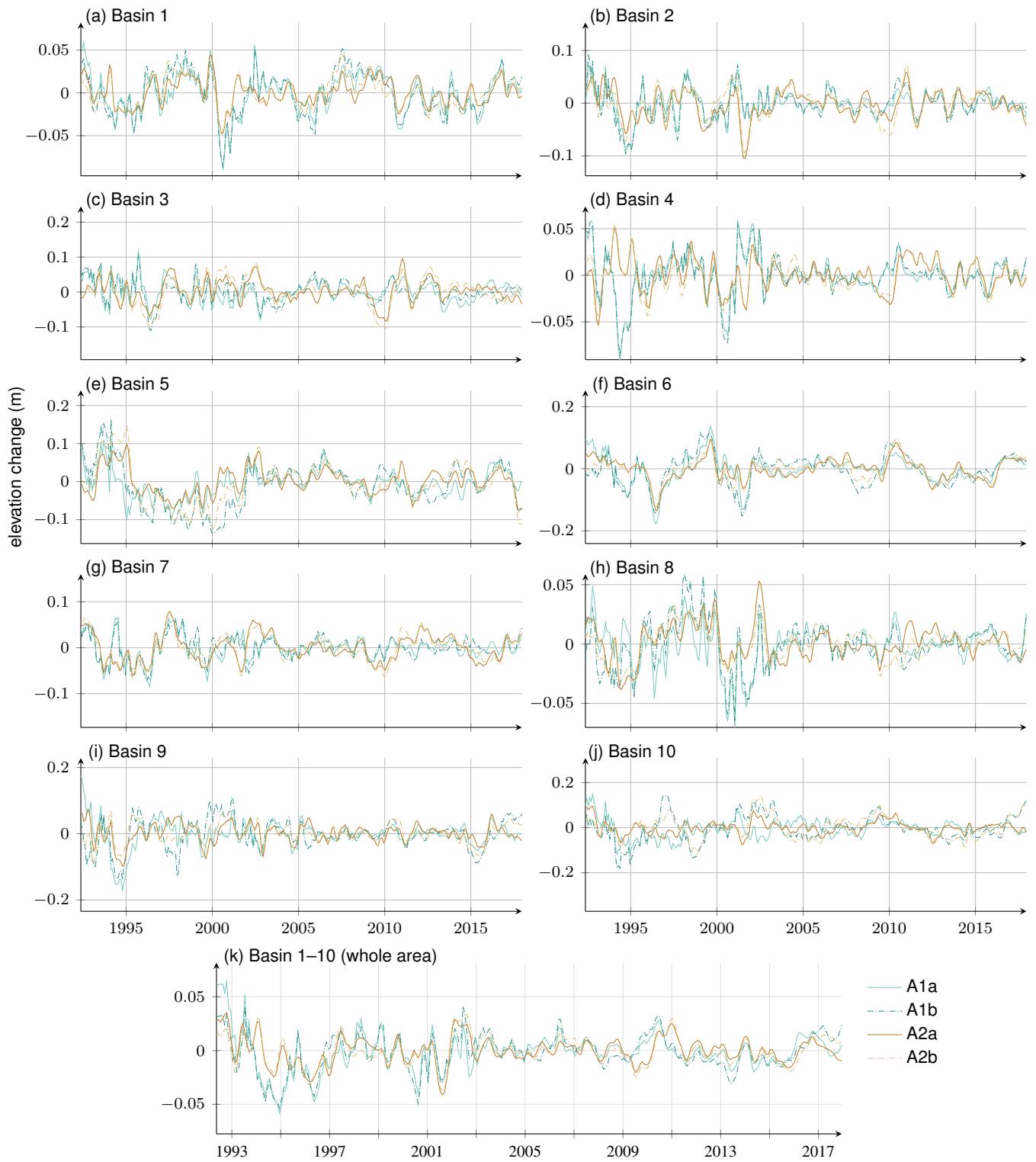
**Figure S24.** Basin mean time series of the altimetric residuals ($r^{\mathrm{A1a}}$, $r^{\mathrm{A2a}}$, $r^{\mathrm{A1b}}$, $r^{\mathrm{A2b}}$).
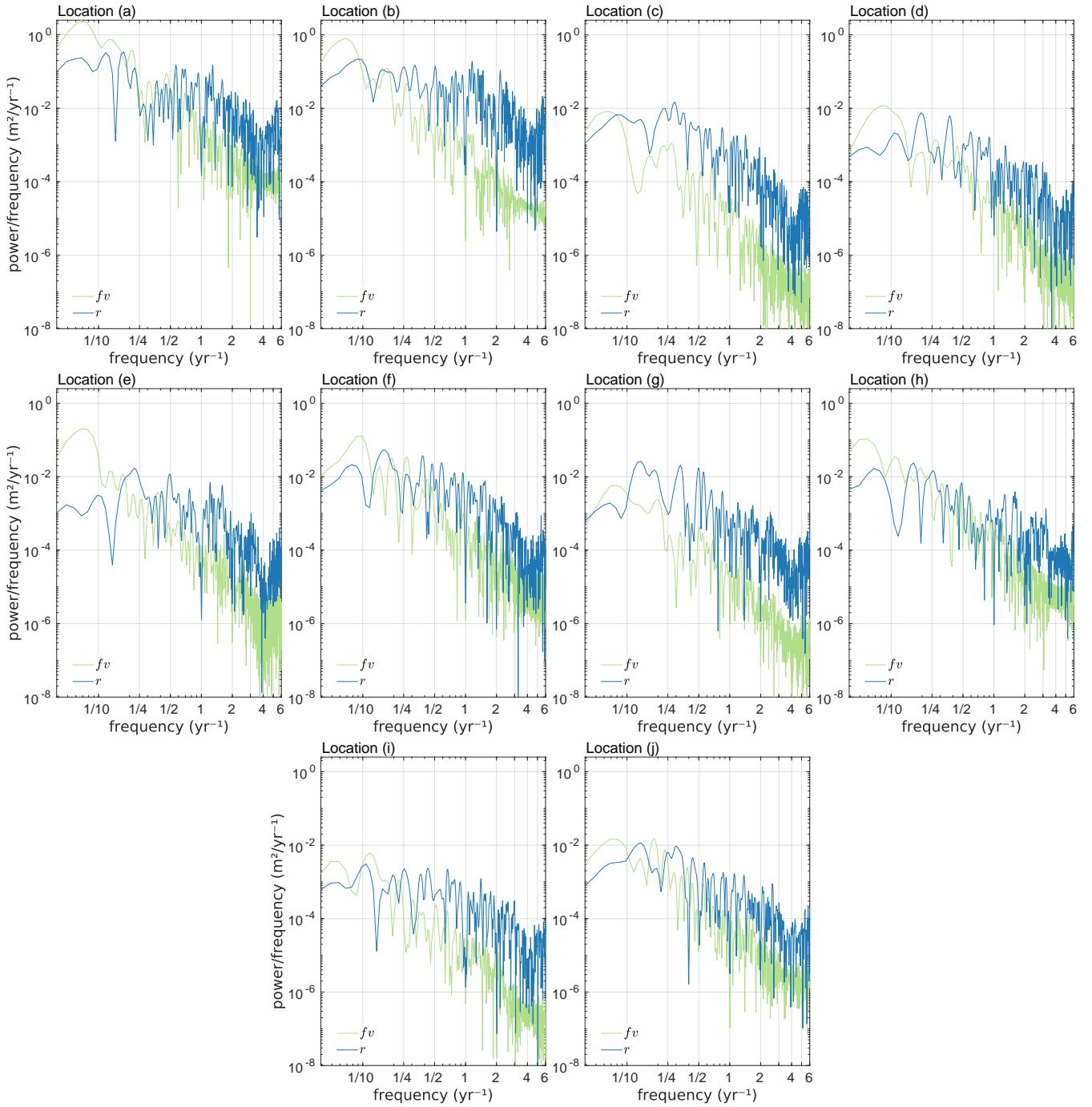
**Figure S25.** For the subset of selected grid points a–j (Fig. 8), Lomb-Scargle power spectral density (psd) of the altimetric residuals $r^{A1a}$ (blue) and the adjusted firn thickness variations $fv^{A1a}$ (green) based on TUD altimetry.
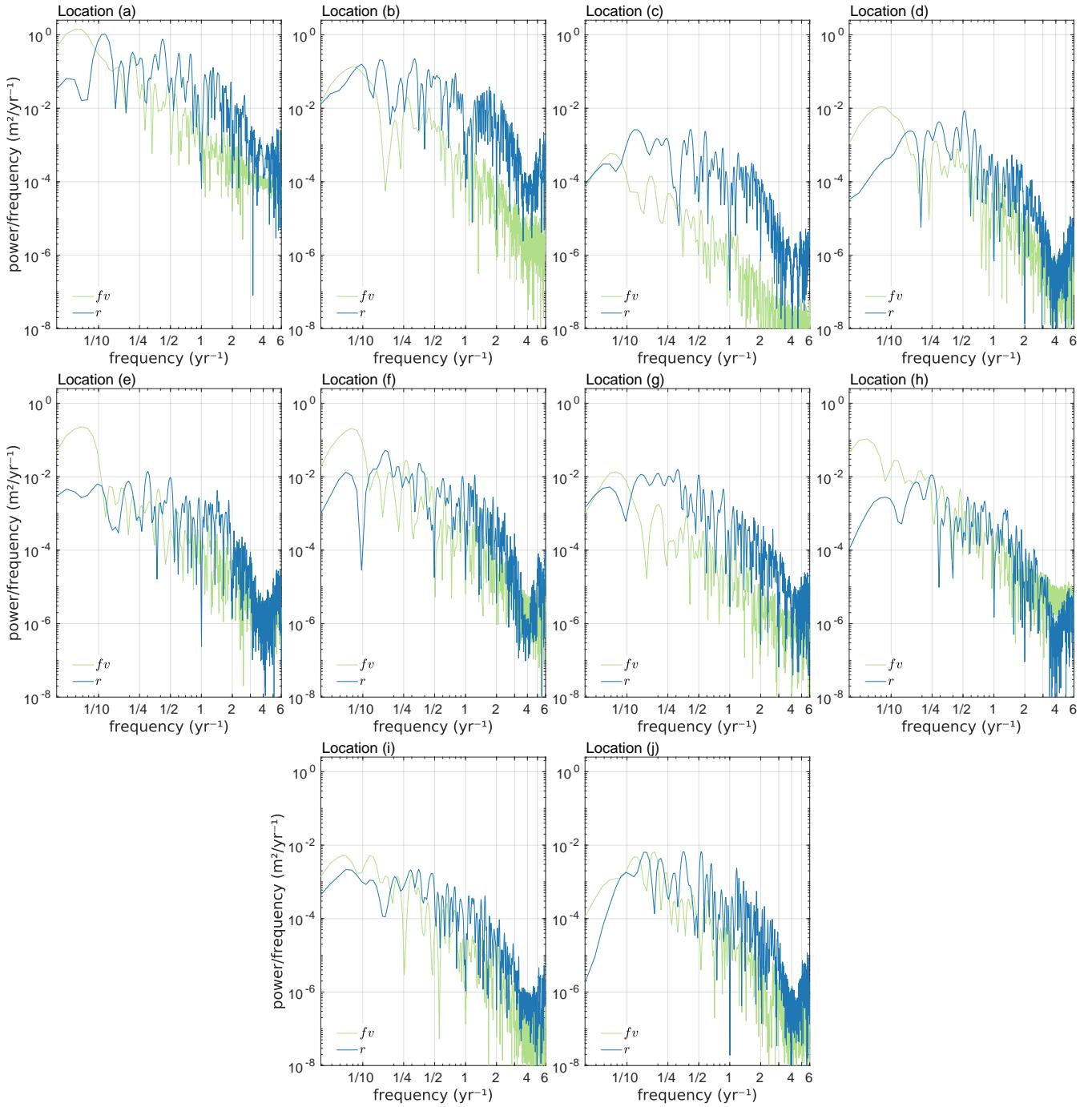
**Figure S26.** For the subset of selected grid points a–j (Fig. 8), Lomb-Scargle power spectral density (psd) of the altimetric residuals $r^{A2a}$ (blue) and the adjusted firn thickness variations $fv^{A2a}$ (green) based on JPL altimetry.
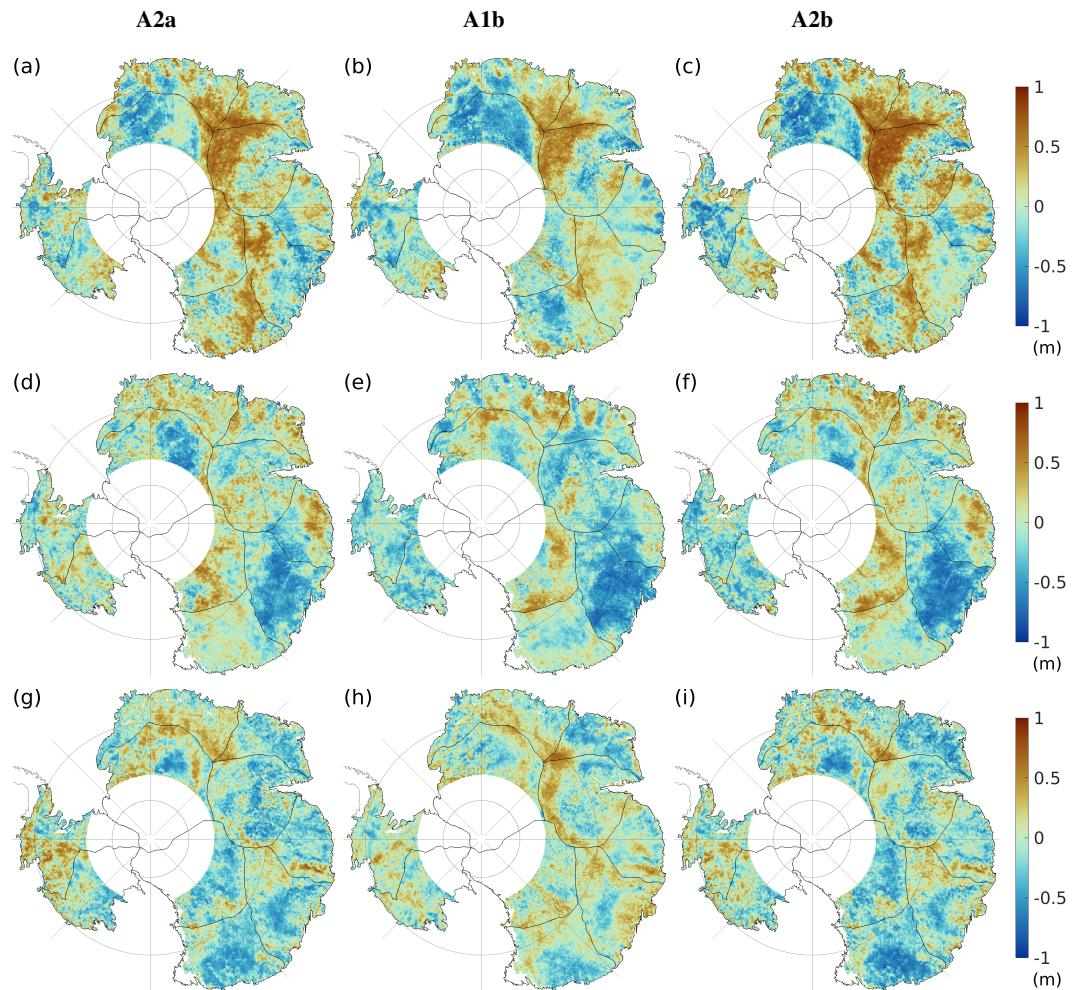
**Figure S27.** PCA results of standardised altimetric residuals. First three EOFs for $r^{\text{A1b}}$ (1st column), $r^{\text{A2a}}$ (2nd column) and $r^{\text{A2b}}$ (3rd column).
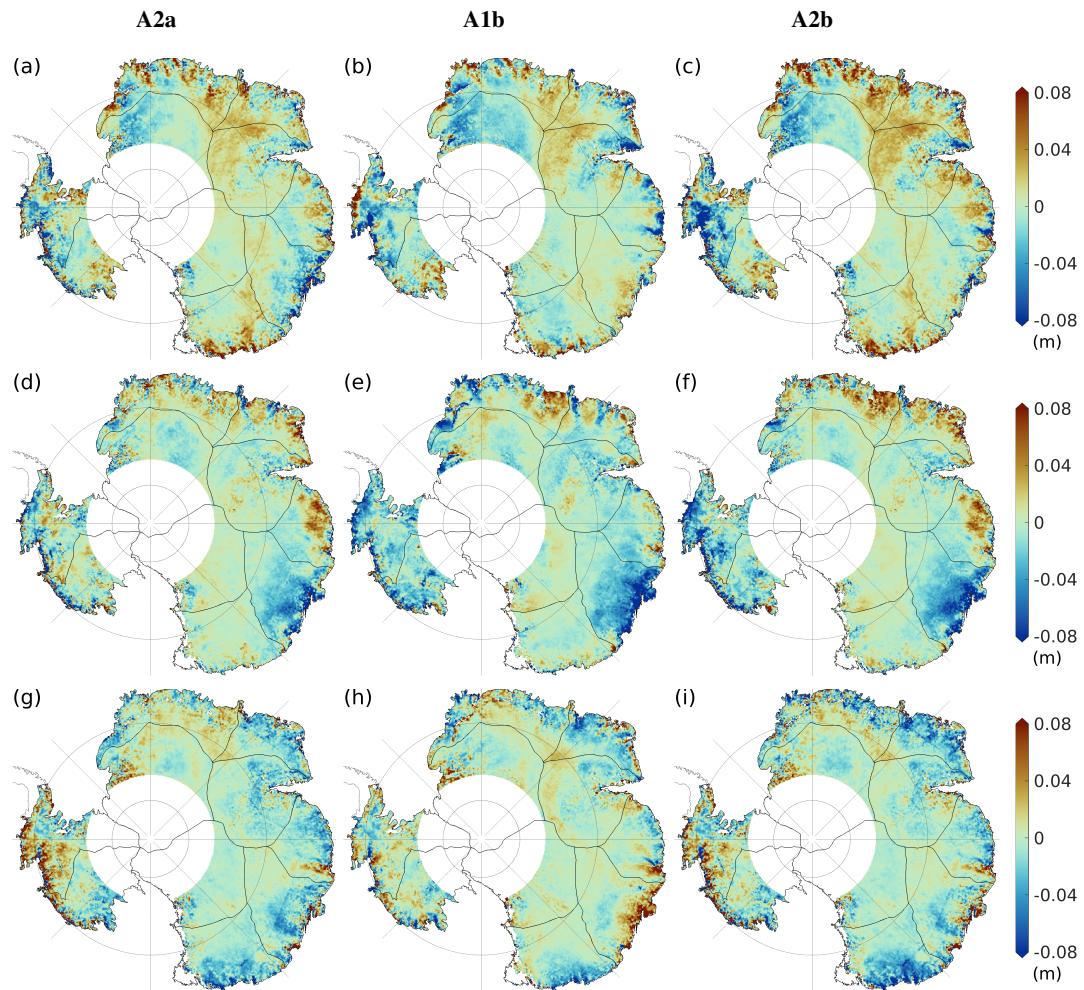
**Figure S28.** PCA results of standardised altimetric residuals. Rescaled first three EOFs for $r^{\mathrm{A1b}}$ (1st column), $r^{\mathrm{A2a}}$ (2nd column) and $r^{\mathrm{A2b}}$ (3rd column).
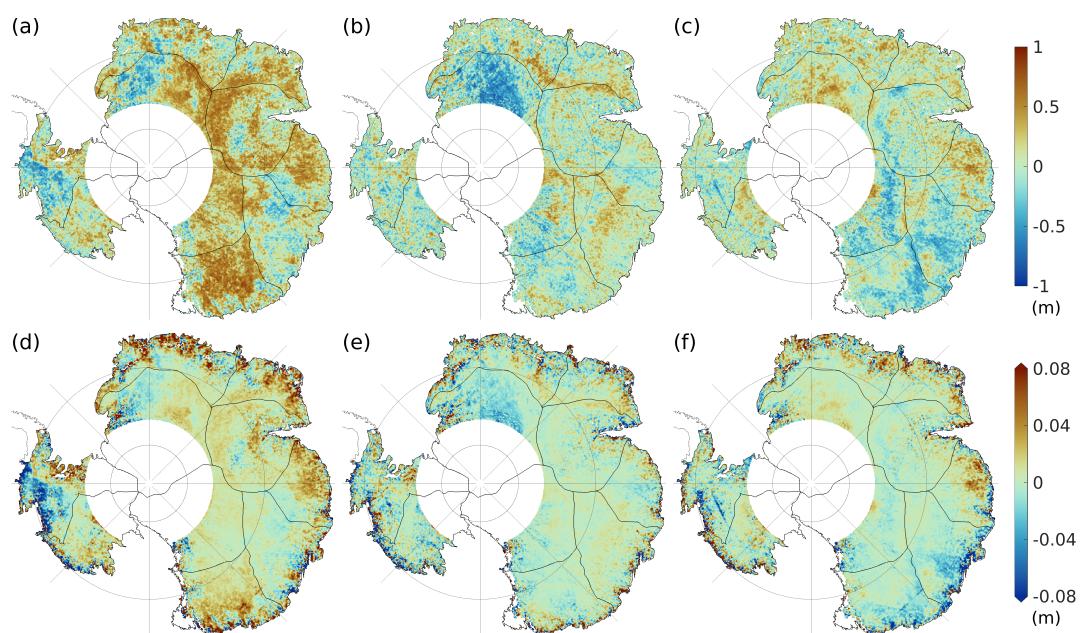
**Figure S29.** PCA results of standardised altimetric residual differences. (a–c) First three EOFs for $r^{\text{A1a}} - r^{\text{A2a}}$. (d–f) Rescaled first three EOFs for $r^{\text{A1a}} - r^{\text{A2a}}$.
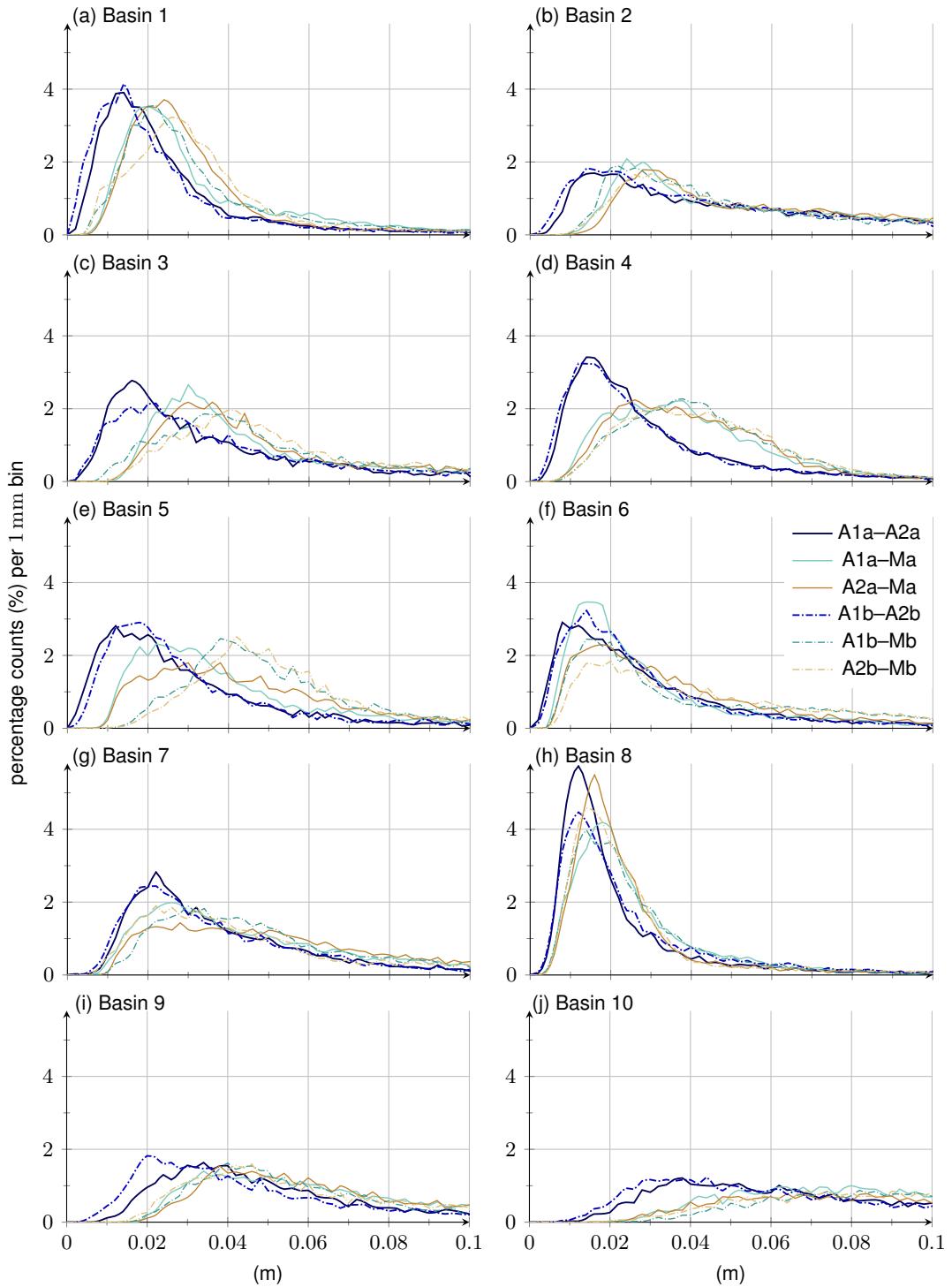
**Figure S30.** Histograms of the temporal rms of differences between various versions of firn thickness variations based on Ma (solid lines) and Mb (dash-dotted line) for all basins.
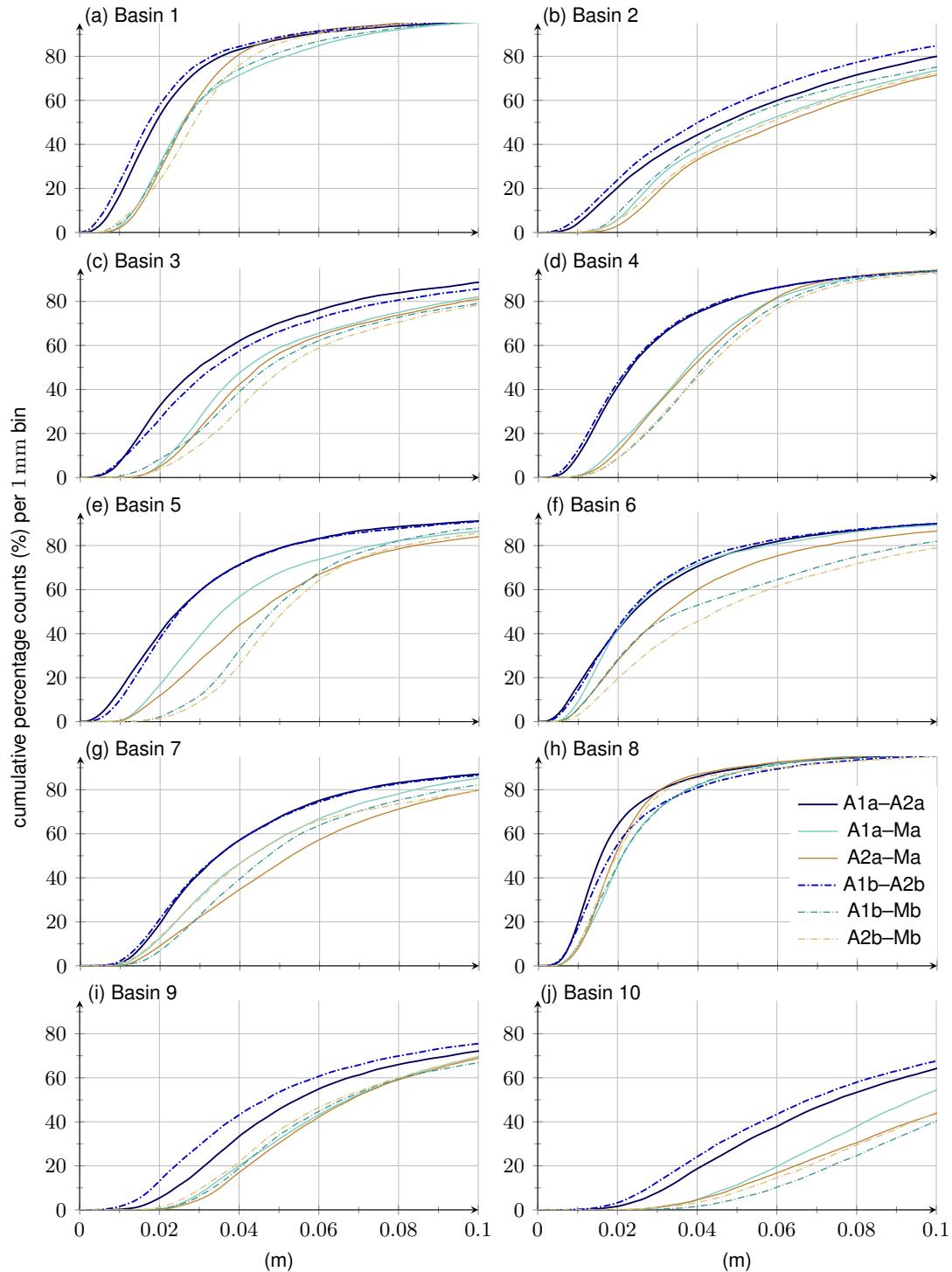
**Figure S31.** Cumulative histograms of the temporal rms of differences between various versions of firn thickness variations based on Ma (solid lines) and Mb (dash-dotted line) for all basins.
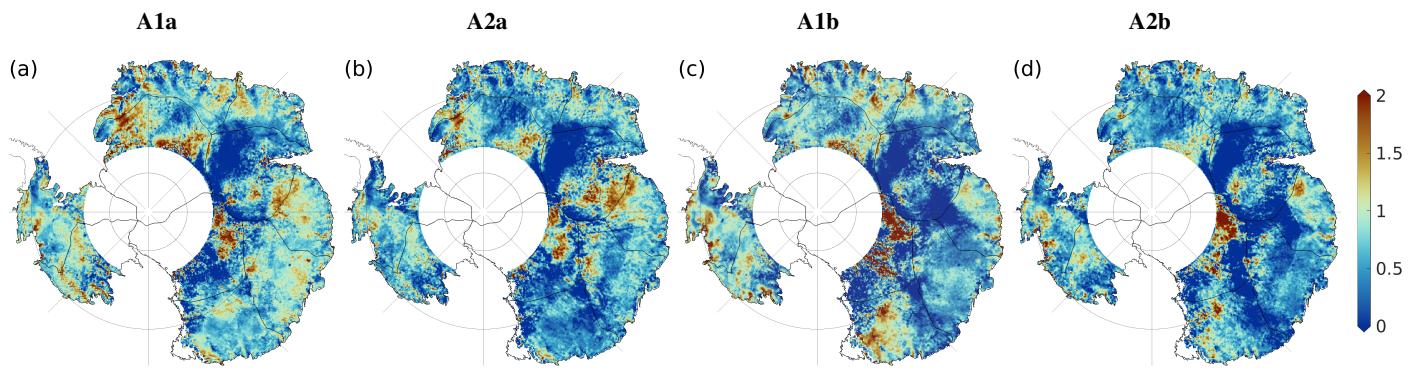
**Figure S32.** Simple scaling factor $e$ adjusted during the regression approach after experiment E2 Eq. A3 (Section A) based on (a) A1a, (b) A2a, (c) A2a and (d) A2b.

## References

Medley, B., Neumann, T., Zwally, H., Smith, B., and Stevens, C.: Simulations of firn processes over the Greenland and Antarctic ice sheets: 1980-2021, The Cryosphere, 16, 3971–4011, https://doi.org/10.5194/tc-16-3971-2022, 2022.

Nilsson, J., Gardner, A., and Paolo, F.: Elevation change of the Antarctic Ice Sheet: 1985 to 2020, Earth System Science Data, 14, 3573–3598, https://doi.org/10.5194/essd-14-3573-2022, 2022.

Rignot, E., Mouginot, J., and Scheuchl, B.: Ice Flow of the Antarctic Ice Sheet, Science, 333, 1427–1430, https://doi.org/10.1126/science.1208336, 2011a.

Rignot, E., Mouginot, J., and Scheuchl, B.: Antarctic grounding line mapping from differential satellite radar interferometry, Geophys. Res. Lett., 38, https://doi.org/10.1029/2011GL047109, 2011b.

Schröder, L., Horwath, M., Dietrich, R., Helm, V., van den Broeke, M., and Ligtenberg, S.: Four decades of Antarctic surface elevation changes from multi-mission satellite altimetry, The Cryosphere, 13, 427–449, https://doi.org/10.5194/tc-13-427-2019, 2019.

Veldhuijsen, S., van de Berg, W., Brils, M., Kuipers Munneke, P., and van den Broeke, M.: Characteristics of the 1979–2020 Antarctic firn layer simulated with IMAU-FDM v1.2A, The Cryosphere, 17, 1675–1696, https://doi.org/10.5194/tc-17-1675-2023, 2023.